



# Multiple genetic paths including massive gene amplification allow *Mycobacterium tuberculosis* to overcome loss of ESX-3 secretion system substrates

Lin Wang<sup>a</sup>, Emmanuel Asare<sup>b</sup>, Amol C. Shetty<sup>c</sup>, Freddy Sanchez-Tumbaco<sup>a</sup>, Megan R. Edwards<sup>a</sup>, Rajagopalan Saranathan<sup>b</sup>, Brian Weinrick<sup>b,d</sup>, Jiayong Xu<sup>b</sup>, Bing Chen<sup>b</sup>, Angèle Bénard<sup>e</sup>, Gordon Dougan<sup>e</sup>, Daisy W. Leung<sup>f</sup>, Gaya K. Amarasinghe<sup>g</sup>, John Chan<sup>b,h</sup>, Christopher F. Basler<sup>a,1</sup>, William R. Jacobs Jr.<sup>b,2</sup>, and JoAnn M. Tufariello<sup>a,1,2</sup>

<sup>a</sup>Center for Microbial Pathogenesis, Institute for Biomedical Sciences, Georgia State University, Atlanta, GA 30303; <sup>b</sup>Department of Microbiology and Immunology, Albert Einstein College of Medicine, Bronx, NY 10461; <sup>c</sup>Institute for Genome Sciences, University of Maryland School of Medicine, Baltimore, MD 21201; <sup>d</sup>Trudeau Institute, Saranac Lake, NY 12983; <sup>e</sup>Wellcome Sanger Institute, Wellcome Genome Campus, Hinxton, Cambridge CB10 1SA, United Kingdom; <sup>f</sup>Division of Infectious Diseases, John T. Milliken Department of Medicine, Washington University in St. Louis School of Medicine, St. Louis, MO 63110; <sup>g</sup>Department of Pathology and Immunology, Washington University in St. Louis School of Medicine, St. Louis, MO 63110; and <sup>h</sup>Department of Medicine, Albert Einstein College of Medicine, Bronx, NY 10461

Contributed by William R. Jacobs Jr.; received July 16, 2021; accepted December 18, 2021; reviewed by Roland Brosch, Keith Derbyshire, and Kyu Rhee

***Mycobacterium tuberculosis* (*Mtb*) possesses five type VII secretion systems (T7SS), virulence determinants that include the secretion apparatus and associated secretion substrates. *Mtb* strains deleted for the genes encoding substrates of the ESX-3 T7SS, *esxG* or *esxH*, require iron supplementation for in vitro growth and are highly attenuated in vivo. In a subset of infected mice, suppressor mutants of *esxG* or *esxH* deletions were isolated, which enabled growth to high titers or restored virulence. Suppression was conferred by mechanisms that cause overexpression of an ESX-3 paralogous region that lacks genes for the secretion apparatus but encodes *EsxR* and *EsxS*, apparent ESX-3 orphan substrates that functionally compensate for the lack of *EsxG* or *EsxH*. The mechanisms include the disruption of a transcriptional repressor and a massive 38- to 60-fold gene amplification. These data identify an iron acquisition regulon, provide insight into T7SS, and reveal a mechanism of *Mtb* chromosome evolution involving “accordion-type” amplification.**

*Mycobacterium tuberculosis* | type VII secretion system | ESX-3 | genetic accordion | TetR-family transcriptional regulator

The major human pathogen, *Mycobacterium tuberculosis* (*Mtb*), causes tuberculosis in 10.4 million people annually, resulting in 1.4 million deaths (1). Significant gaps remain in our understanding of *Mtb* pathogenesis. Type VII secretion systems (T7SS) are an important, but incompletely understood class of *Mtb* virulence determinants that have been explored as targets for novel chemotherapies (2) and manipulated to generate attenuated vaccines (3–5). *Mtb* encodes five T7SS in genomic loci, designated *esx-1* through *esx-5* (6). Each of these loci encodes the secretion apparatus itself and associated substrates, including pairs of small helical proteins belonging to the WXG100 family, containing a Trp-Xaa-Gly (WXG) motif (7), as well as members of the proline-glutamic acid (PE) and proline-proline-glutamic acid (PPE) families (8). ESX-1 is the best studied of the *Mtb* T7SS. It modulates host signaling pathways, bacterial trafficking, and promotes virulence (9–13). However, the mechanisms by which individual protein substrates contribute to ESX functions remain incompletely understood.

The *esx-3* locus encodes the secretion apparatus as well as the WXG100 pair *EsxG/EsxH* and a pair of PE/PPE protein family members, PE5/PPE4 (6). The *esx-3* gene cluster (*rv0282-rv0292*) is regulated by the iron-dependent transcriptional repressor, IdeR (14), the zinc uptake regulator, Zur (15), the manganese transport regulator, MntR (16), and in *Mycobacterium bovis* may respond to oxidative stress through interactions between the CmtR regulator and Zur (17). Genetic studies implicate ESX-3 in mycobacterial utilization of iron bound to the siderophores mycobactin and carboxymycobactin (18–23). Whereas *esx-3* was

previously thought to be essential for growth, *esx-3* deletion strains are in fact recoverable in medium supplemented with various iron complexes, whether the deletions encompass individual *esx-3* genes or the full operon (22). In addition, evidence from studies of deletion mutants suggests that ESX-3 also plays iron-independent roles in *Mtb* pathogenesis. Notably, *EsxH* interacts with the host cell endosomal sorting complex required for transport (ESCRT) machinery, impairing the capacity of effector CD4<sup>+</sup> T cells to target infected macrophages and clear *Mtb* infection (24). Additionally, *EsxH* is a T cell antigen that may serve as an immunological decoy. In mouse models, *EsxH* elicits robust CD8<sup>+</sup> T cell responses, which fail to effectively recognize *Mtb*-infected macrophages (25).

## Significance

The *Mycobacterium tuberculosis* (*Mtb*) ESX-3 type VII secretion system plays a critical role in iron acquisition. Infection of mice with highly attenuated *Mtb* deletion mutants lacking *esxG* or *esxH*, genes encoding key ESX-3 substrates, unexpectedly yielded suppressor mutants with restored capacity to grow in vivo and in vitro in the absence of iron supplementation. Whole-genome sequencing identified two mechanisms of suppression, the disruption of a transcriptional repressor that regulates expression of an ESX-3 paralogous region encoding *EsxR* and *EsxS*, and a massive 38- to 60-fold gene amplification of this same region. These data are significant because they reveal a previously unrecognized iron acquisition regulon and inform mechanisms of *Mtb* chromosome evolution.

Author contributions: D.W.L., G.K.A., C.F.B., W.R.J., and J.M.T. designed research; L.W., E.A., F.S.-T., M.R.E., R.S., B.W., J.X., B.C., A.B., D.W.L., G.K.A., and J.M.T. performed research; L.W., E.A., A.C.S., M.R.E., R.S., B.W., A.B., D.W.L., G.K.A., J.C., C.F.B., W.R.J., and J.M.T. analyzed data; G.D., D.W.L., G.K.A., J.C., C.F.B., W.R.J., and J.M.T. provided project oversight and supervision; C.F.B., W.R.J., and J.M.T. wrote and edited the manuscript with input from all authors.

Reviewers: R.B., Institut Pasteur; K.D., Wadsworth Center, New York State Department of Health; and K.R., Cornell University.

The authors declare no competing interest.

This article is distributed under Creative Commons Attribution-NonCommercial-NoDerivatives License 4.0 (CC BY-NC-ND).

<sup>1</sup>Present address: Department of Microbiology, Icahn School of Medicine at Mount Sinai, New York, NY 10029.

<sup>2</sup>To whom correspondence may be addressed. Email: william.jacobs@einsteinmed.edu or joann.tufariello@mssm.edu.

This article contains supporting information online at <http://www.pnas.org/lookup/suppl/doi:10.1073/pnas.2112608119/-DCSupplemental>.

Published February 22, 2022.

Previous work demonstrated that *Mtb* strains bearing deletions of the entire *esx-3* region or of the *esxH* gene alone are highly attenuated in their capacity to cause disease in immunocompetent mice (22). Here, we describe how a subset of immunocompetent mice infected with  $\Delta esxG/\Delta esxH$  mutants exhibited unexpectedly higher bacterial burdens or early mortality. The bacteria recovered from these mice no longer required iron supplementation in the form of hemin or mycobactin for in vitro growth. Whole-genome sequencing (WGS) of the in vivo isolates identified two general classes of suppressor mutations associated with these phenotypes. These include mutations in the putative transcriptional repressor protein Rv3058c, which is thought to regulate expression of a locus encoding several PE/PPE proteins and EsxR/EsxS, a WXG100 pair with high identity to EsxH/EsxG. The second class was a remarkable 38- to 60-fold gene amplification of *esxR/esxS* and flanking *pe/ppc* genes, involving a tandem duplication of a 2,440-bp region. These data implicate Rv3058c and the locus encoding EsxR/EsxS as a previously unrecognized iron regulon and point to a remarkable genetic plasticity of *Mtb*, which allows it to overcome impediments to in vivo growth and virulence.

## Results

**Isolation of  $\Delta esxG$  and  $\Delta esxH$  Phenotypic Revertants In Vitro and In Vivo.** The in vitro iron-related growth phenotypes of  $\Delta esx-3$ ,  $\Delta esxH$ , and  $\Delta esxG$  are similar in that none of the mutants grow effectively on standard 7H10 medium, and all require supplementation with iron complexes, such as mycobactin J or hemin, for growth (22). Furthermore, *Mtb*  $\Delta esx-3$  region mutants and  $\Delta esxH$  mutants are highly attenuated in vivo. Following aerosol infection of C57BL/6 mice, bacteria failed to proliferate in lungs, and dissemination to the spleen was not observed (22). Based on these findings,  $\Delta esxG$  strains were expected to behave similarly after aerosol infection of C57BL/6 mice. Instead, we found that at 3 wk postinfection, two of four  $\Delta esxG$ -infected mice had very low lung CFU levels ( $\sim 10^2$  CFU), indicating the absence of growth, while the other two mice had bacterial burdens several logs higher, approximating those of mice infected with WT or  $\Delta esxG$ -complemented strains ( $\sim 10^5$  CFU) (Fig. 1A). A similar dichotomy was evident at the 8-wk and 16-wk harvests for the  $\Delta esxG$ -infected mice. Dissemination to spleens was also observed in the  $\Delta esxG$ -infected mice that exhibited elevated pulmonary bacterial burdens (Fig. 1A).

Bacteria were recovered from the lungs and spleens of those  $\Delta esxG$ -infected mice that exhibited high bacterial titers. These isolates were found to have acquired the capacity to grow on standard 7H10 medium in the absence of supplementation with mycobactin J (Fig. 1B). This growth phenotype contrasted with that of the  $\Delta esxG$  and  $\Delta esxH$  parental strains, which formed colonies on 7H10 supplemented with 200 ng/mL mycobactin J, but not on standard 7H10 medium, as previously reported (22) and as demonstrated in Fig. 1B. In a prior study, growth to high titers by  $\Delta esxH$  was not observed in C57BL/6 mice following aerosol infection (22). In this study, CBA mice were chosen for infection by  $\Delta esxH$  because these mice exhibit a greater susceptibility to infection with *Mtb* (26–30). Following intravenous infection of five CBA mice with  $\Delta esxH$ , early morbidity was observed for one mouse, which succumbed  $\sim 100$  d prior to the remaining  $\Delta esxH$ -infected mice (Fig. 1C). Notably, bacteria recovered from the lungs of this mouse had also acquired the capacity to grow on standard 7H10 medium lacking mycobactin J (Fig. 1B).

**Phenotypic Revertants Harbor Mutations in Rv3058c, a Putative TetR-Family Regulator Implicated in *esxR/esxS* Expression.** Given that the  $\Delta esxG$  and  $\Delta esxH$  isolates exhibited altered growth properties following in vivo passage, we hypothesized that they acquired genetic differences resulting in suppressor phenotypes. Following in vitro culturing, complete genome sequences were

determined for the  $\Delta esxG$  parent, the  $\Delta esxG$  strains with putative suppressor mutations, and our laboratory strain of H37Rv WT. Sequenced isolates included  $\Delta esxG$  recovered from C57BL/6 mice at 8 wk and 16 wk post-aerosol infection and are detailed in *SI Appendix, Table S1*.

Given the reversion of  $\Delta esxG$  growth phenotypes in some mice, it was also of interest to attempt isolation of potential revertants in vitro. Large numbers of  $\Delta esxG$  were plated onto 7H11 medium without additional iron supplements, resulting in the appearance of two large colonies, which were also subjected to WGS (*SI Appendix, Table S1*). Like the suppressor strains recovered from the in vivo studies, these in vitro suppressor strains also grew like WT in replating studies, exhibiting growth on 7H10 medium in the absence of mycobactin (Fig. 1B).

WGS confirmed the presence of the complete *esxG* coding sequence in the WT strain and the  $\sim 180$ -bp deletion within the  $\Delta esxG$  parent, as well as the various  $\Delta esxG$  suppressor mutants (*SI Appendix, Fig. S1*). Sequencing data were further analyzed to identify the SNPs with the highest variant frequencies specific to the suppressor isolates, as these were thought most likely to represent the genetic changes responsible for the suppressor phenotypes. High-confidence SNPs with frequencies higher than 90% that were present in the putative  $\Delta esxG$  suppressor mutants but absent from both H37Rv WT and the  $\Delta esxG$  parent are summarized in *SI Appendix, Table S2*, with additional details in *SI Appendix, Table S1* and *Dataset S1*.

One SNP mutation (SNP\_1) (*SI Appendix, Table S2*) was shared by several in vivo suppressor strains that were isolated from organs of  $\Delta esxG$ -infected mice with the highest bacterial titers, including a lung isolate obtained at 8 wk postinfection ( $\Delta esxG$  in vivo-1), and two lung isolates obtained at 16 wk postinfection from the same mouse ( $\Delta esxG$  in vivo-2 and -3) (*SI Appendix, Table S1*). SNP\_1 is a missense mutation in the *rv3058c* gene, resulting in the substitution of histidine for arginine at position 31 (R31H) of the encoded protein. SNP\_1 was also present in the large colonies isolated in vitro following plating of  $\Delta esxG$  on 7H11 medium in the absence of mycobactin J ( $\Delta esxG$  in vitro-1 and -2) (*SI Appendix, Table S1*).

Given that a mutation in *rv3058c* was associated with growth recovery of  $\Delta esxG$  in vivo and in vitro, targeted PCR amplification and Sanger sequencing of the *rv3058c* gene was pursued in a variety of additional samples (*SI Appendix, Tables S1 and S2*). These included isolates from the lungs and spleens of  $\Delta esxG$ -infected mice obtained at 8 and at 16 wk postinfection. This identified multiple isolates with the R31H change within *rv3058c* (SNP\_1) (*SI Appendix, Table S1*). We also identified a different *rv3058c* mutation, SNP\_2 resulting in aspartic acid for histidine at position 22 (H22D), in two isolates from the spleen of a  $\Delta esxG$ -infected mouse (*SI Appendix, Tables S1 and S2*).

The *rv3058c* genes of multiple bacterial isolates from the  $\Delta esxH$ -infected CBA mouse exhibiting early morbidity were also examined. These isolates (strains  $\Delta esxH$  in vivo-1 to in vivo-8) (*SI Appendix, Tables S1 and S2*), recovered from lung, spleen, and liver, all shared SNP\_3, resulting in the substitution of a proline for a leucine at position 33 (L33P) of Rv3058c. It should be noted that for mice in which multiple isolates were examined, including from different organs, only a single high-frequency SNP was identified per mouse (*SI Appendix, Table S1*). Additionally, representative isolates containing each *rv3058c* mutation that was identified, SNP\_1, SNP\_2, and SNP\_3 were plated on media lacking mycobactin supplementation, and all exhibited restoration of growth (Fig. 1B).

**Mutations in Rv3058c Map to a Putative DNA-Binding Domain and Disrupt DNA Binding.** The *rv3058c* gene is predicted to encode a member of the TetR family of transcriptional regulators, most of which function as transcriptional repressors, with the suppression of transcription relieved upon binding of a ligand (31,

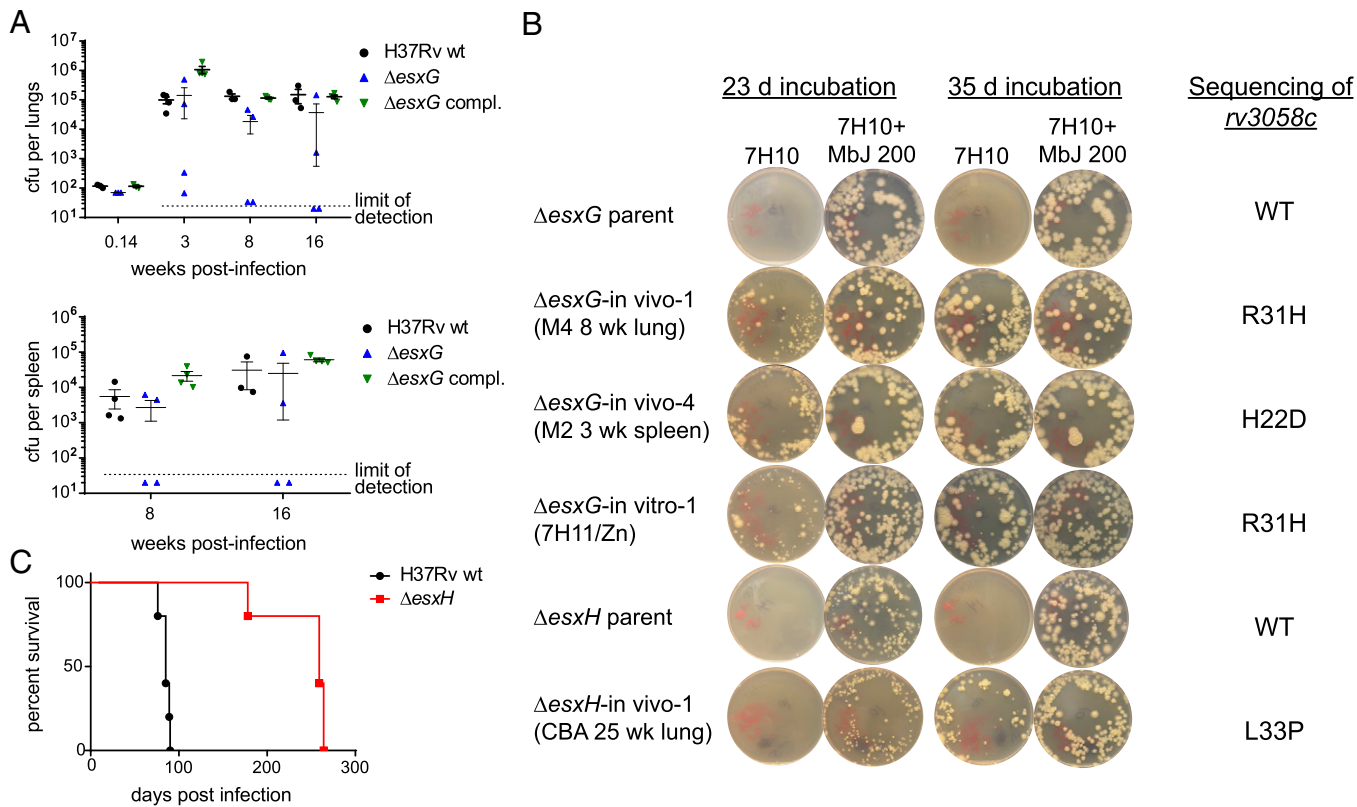


**Fig. 1.**  $\Delta$ esxG and  $\Delta$ esxH recovered from mice form colonies on plain 7H10 and harbor point mutations in *rv3058c*. (A) C57BL/6 mice were infected by aerosol with H37Rv WT, the  $\Delta$ esxG unmarked strain ( $mc^27845$ ), and  $\Delta$ esxG complemented with an integrating vector expressing *esxGH* ( $mc^27866$ ). Lung CFU were determined at 24 h and at 3, 8, and 16 wk postinfection and spleen CFU were determined at 8 and 16 wk postinfection.  $n = 3$  to 4 mice per group. Mean  $\pm$  SEM are indicated. Dotted line denotes limit of detection. The H37Rv WT group CFU data were previously reported in comparison with  $\Delta$ mbtB,  $\Delta$ esxH, and  $\Delta$ ppe5-ppe4 strains (22). The  $\Delta$ esxG mutant and complemented strains tested in the present study were included in the same experiment but not previously reported. (B) The indicated isolates recovered after in vivo growth were plated onto 7H10 medium with and without 200 ng/mL mycobactin J, in comparison with parental strains. Results of sequencing analysis within the *rv3058c* gene as compared with the parental strain are shown at right. (C) CBA mice were intravenously infected with indicated strains and survival was monitored.  $n = 5$  mice per group. The H37Rv WT group survival data were previously reported in comparison with  $\Delta$ mbtB and  $\Delta$ ppe5-ppe4 (22). The  $\Delta$ esxH mutant tested in the present study was included in the same experiment but not previously reported.

32). TetR-family regulators contain conserved helix–turn–helix motifs at their N termini, which function in DNA binding, whereas the C terminus contains the ligand-binding pocket (31–33). As the suppressor mutations H22D, R31H, and L33P all mapped near the 5' end of *rv3058c*, we hypothesized that they impair DNA binding. Both the Tuberculosis Database and published data, including chromatin immunoprecipitation-sequencing (ChIP-seq) analysis, predict three binding sites for Rv3058 (34–36): one in the intergenic region between *rv3023c* and *pe29*; another in the intergenic region between *rv0834c* and *rv0835*; and third, an intragenic site within the *rv0869c* gene. The two intergenic regions were used in EMSAs and reporter assays to characterize Rv3058c–DNA interactions, including the effects of the N-terminal amino acid substitutions on DNA binding.

Recombinant Rv3058c WT protein was expressed in *Escherichia coli* and purified (SI Appendix, Fig. S2A). The cy5-labeled DNA probes comprising the promoter regions upstream of *rv0834c* and *pe29* were both found to be shifted markedly by the addition of recombinant purified Rv3058c WT protein (SI Appendix, Fig. S2B, Left). After visualization of the cy5 signal, the gel was stained with Imperial blue protein stain (SI Appendix, Fig. S2B, Right), revealing that Rv3058c WT protein comigrated with the shifted DNA probe, providing further evidence for their interaction. Using EMSA, we were unable to assess the DNA-binding properties of the Rv3058c R31H point mutant or of an

H22D/R31H/L33P triple mutant because the proteins did not enter the gel efficiently, with Imperial blue staining revealing that most of the protein remained at the top of the wells.

For further analysis of Rv3058c interactions with predicted target promoters, a synthetic mammalian gene circuit was employed. It was comprised of a chimeric transcription factor expression plasmid and secreted embryonic alkaline phosphatase (SEAP) reporter plasmids (SI Appendix, Fig. S2C) and was adapted from an approach used to characterize the *Mtb* TetR-family member EthR2 (37). For the transcription factor plasmid, the coding sequence of *Mtb rv3058c* was fused to the herpes simplex VP16 transcription-activating domain in a mammalian expression vector, generating plasmid p3058c-VP16 (SI Appendix, Table S3). In this system, the Rv3058c portion of the chimera should bind to mycobacterial target promoters, and the VP16 domain serves as a transcriptional activator functional in mammalian cells. Constructs were made with WT Rv3058c as well as the R31H point mutant of Rv3058c, which was chosen due to its presence in multiple in vivo and in vitro suppressor isolates (SI Appendix, Table S3).

For the SEAP reporter plasmids, the ~200-bp promoter regions of *rv0834c* and *pe29* were inserted upstream of a minimal variant of the human cytomegalovirus-derived promoter (PhCMVmin) (SI Appendix, Fig. S2C and Table S3). The transcription factor plasmids (Rv3058c WT or R31H mutant) and SEAP reporter plasmids were cotransfected at various ratios

into HEK 293T cells, and SEAP expression was quantified in cell culture supernatants 48 h posttransfection. Controls included individual plasmids, empty vectors (EV), and a positive control vector that constitutively expressed SEAP. Significantly higher levels of SEAP activity were detected with Rv3058c WT than with the R31H mutant for both the *rv0834c* and *pe29* upstream sequences (SI Appendix, Fig. S2C). Western blots verified similar expression for the WT and mutant proteins. Therefore, the results support the ability of Rv3058c to interact with these promoter sequences and provide evidence that the R31H mutation impairs DNA-binding activity.

**Deletion of *rv3058c* Phenocopies the Revertant In Vitro Growth Phenotypes.** Given that missense mutations in Rv3058c were associated with impaired function of the protein, we hypothesized that a deletion mutant of *rv3058c* might phenocopy the suppressor mutants. Therefore, the *rv3058c* coding sequence was deleted from four genetic backgrounds (i.e., H37Rv WT,  $\Delta$ *esxG*,  $\Delta$ *esxH*, and  $\Delta$ *esx-3*) (SI Appendix, Table S4). The deletions were confirmed by three-primer PCR and further verified by WGS using Illumina MiSeq technology, which showed the absence of reads at the relevant loci (SI Appendix, Fig. S3). Growth of the mutant strains was assessed on 7H10 solid media prepared in the absence and presence of mycobactin supplementation. Similar to the  $\Delta$ *esxG* and  $\Delta$ *esxH* revertant strains (Fig. 1B), the  $\Delta$ *esxG*  $\Delta$ *rv3058c* and  $\Delta$ *esxH*  $\Delta$ *rv3058c* double-deletion mutants grew on 7H10 lacking additional iron supplements (Fig. 2A). However, the double  $\Delta$ *esx-3*  $\Delta$ *rv3058c* mutant did not grow in the absence of mycobactin supplementation (Fig. 2A). These data indicate that the phenotypes of the  $\Delta$ *esxG* and  $\Delta$ *esxH* revertants are due to loss-of-function mutations in Rv3058c, but that rescue of the growth phenotype requires the presence of other components of the *esx-3* locus, most likely those that comprise the secretion apparatus.

**Relevance of the Rv3058c-Regulated Genes *esxR* and *esxS* in the Revertant In Vitro Growth Phenotypes.** The WGS data, together with the reporter construct and EMSA results, led us to test whether a genetic locus or loci normally under negative regulation by Rv3058c might be derepressed in the double *rv3058c/esxG* or *rv3058c/esxH* deletion mutants, thereby compensating for the absence of EsxG and EsxH. The putative Rv3058c intergenic binding site found adjacent to *pe29* (*rv3022A*) lies upstream of a locus encoding a pair of *esx* genes, *esxS* and *esxR*, which are flanked by *pe-ppe* genes (referred to here as the “*esxRS* locus,” defined as extending from *pe29* [*rv3022A*] through *esxQ* [*rv3017c*]) (Fig. 2B). Because EsxR and EsxH exhibit substantial homology (84% amino acid identity), as do EsxS and EsxG (92% amino acid identity), this locus was considered to be a strong candidate for providing compensatory functions. Therefore, the effects of overexpression of *esxS/esxR* on the in vitro iron requirements of strains lacking *esxG* and/or *esxH* were investigated. Transformation of H37Rv  $\Delta$ *esxH* or  $\Delta$ *esxGH* with an integrating plasmid (pMV361) expressing *esxG/esxH* under control of the strong, constitutive *hsp60* promoter ( $P_{hsp60}$ ) (38) restored the ability of the strains to grow on 7H10 medium in the absence of iron supplements (Fig. 2B and C). A similar construct expressing *esxS/esxR* was equally effective in restoring growth, indicating the capacity of EsxS/EsxR to complement and substitute for EsxG/EsxH (Fig. 2B and C). Although the  $\Delta$ *esxG*/ $\Delta$ *esxH* strains encode intact copies of *esxS* and *esxR*, the genes are presumably under negative regulation by Rv3058c at their native locus, which is bypassed by placing the genes under the control of  $P_{hsp60}$ .

EsxG and EsxH are secreted via the ESX-3 secretion system, and deletion of the entire *esx-3* region phenocopies the iron-dependent phenotypes of single and double *esxG/esxH* deletion

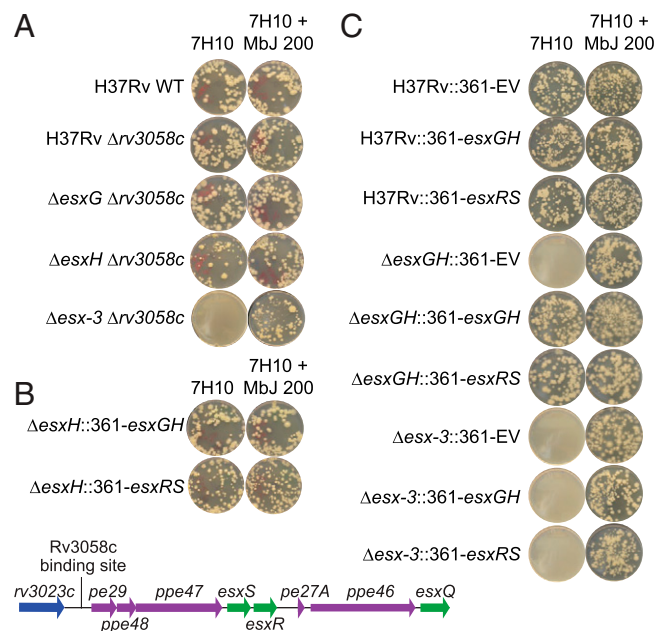


**Fig. 2.** Deletion of *rv3058c* or overexpression of *esxS-esxR* complements in vitro growth defects of *esxG/H* mutant strains. (A) Cultures of double mutants ( $\Delta$ *esxG* $\Delta$ *rv3058c*,  $\Delta$ *esxH* $\Delta$ *rv3058c*, and  $\Delta$ *esx-3* $\Delta$ *rv3058c*) were plated in parallel onto media containing and lacking 200 ng/mL mycobactin J in comparison with the H37Rv WT strain. Deletion of *rv3058c* permits growth of  $\Delta$ *esxG* and  $\Delta$ *esxH* but not  $\Delta$ *esx-3*. (B)  $\Delta$ *esxH* was transformed with pMV361 vector expressing *esxGH* or *esxRS* and selected on kanamycin; equivalent inocula were plated on 7H10 medium with and without mycobactin J. Both constructs rescued growth in the absence of mycobactin J. Below is a schematic illustrating the genomic organization of the *esxRS* locus; the location of the putative Rv3058c binding site upstream of *pe29* is indicated. (C) H37Rv WT,  $\Delta$ *esxGH*, and  $\Delta$ *esx-3* were transformed with pMV361 EV or with pMV361 vector expressing *esxGH* or *esxRS* and selected on kanamycin. Equivalent numbers were plated on media with and without mycobactin J. Both the *esxGH*- and the *esxRS*-expressing constructs but not the EV rescued growth of  $\Delta$ *esxGH* on standard 7H10 lacking mycobactin J. In contrast, growth of  $\Delta$ *esx-3* was not rescued by any of the constructs.

mutants (22). To determine whether complementation with *esxS-esxR* requires an intact ESX-3 secretion system, plasmids expressing *esxG/esxH* or *esxS/esxR* were introduced into a  $\Delta$ *esx-3* strain and plated on 7H10 medium lacking additional iron supplements (Fig. 2C). No growth was detected in the resulting strains,  $\Delta$ *esx-3*::361-*esxGH* and  $\Delta$ *esx-3*::361-*esxRS*, in the absence of iron supplementation, although each strain grew in the presence of mycobactin J. These data support the notion that both of these Esx heterodimeric pairs require an intact ESX-3 secretion system for their function (22, 39, 40).

**Deletion of *rv3058c* or Overexpression of *esxS/esxR* Restores Virulence In Vivo.** After confirming that deletion of *rv3058c* or overexpression of *esxS/esxR* corrected the in vitro iron-related growth defects of *esxG* and *esxH* deletion mutants, the effects of these genetic manipulations on virulence were examined by employing mouse models used previously to study in vivo behavior of the deletion mutants (22). In the first model, intravenous infection of severe combined immunodeficiency (SCID) mice, revealed that deletion of *rv3058c* reversed the attenuation of the  $\Delta$ *esxG* and  $\Delta$ *esxH* parental strains (an attenuation that was mild for the  $\Delta$ *esxG* parent, and more marked for the  $\Delta$ *esxH* parent), mimicking findings observed for the Rv3058c N-terminal point mutants tested in parallel ( $\Delta$ *esxG* Rv3058c H22D,  $\Delta$ *esxG* Rv3058c R31H and  $\Delta$ *esxH* Rv3058c L33P) (Fig. 3A and B). Deletion of *rv3058c* from the parental H37Rv WT strain did

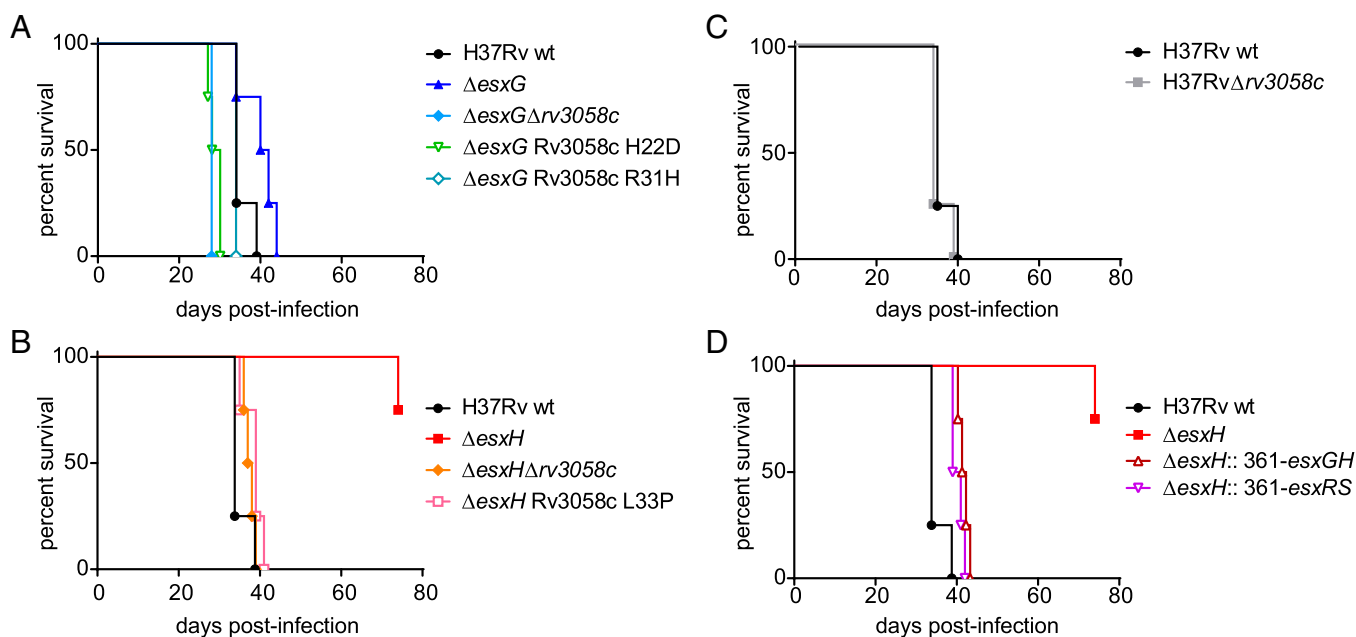


**Fig. 3.** Restoration of virulence of  $\Delta esxG$  and  $\Delta esxH$  strains by mutation of *rv3058c* or forced expression of *esxRS*. (A) Percent survival over time of SCID mice infected by the intravenous route with H37Rv WT,  $\Delta esxG$ ,  $\Delta esxG \Delta rv3058c$ , or  $\Delta esxG$  Rv3058c H22D or R31H point mutants. Similar experiments were performed but with H37Rv WT,  $\Delta esxH$ ,  $\Delta esxH \Delta rv3058c$ , or  $\Delta esxH$  Rv3058c L33P point mutant (B), with H37Rv WT or H37Rv  $\Delta rv3058c$  (C), and with H37Rv WT,  $\Delta esxH$ ,  $\Delta esxH$  stably transformed with a plasmid that expresses *esxG* and *esxH* ( $\Delta esxH::361-esxGH$ ) or  $\Delta esxH$  stably transformed with a plasmid that expresses *esxS* and *esxR* ( $\Delta esxH::361-esxRS$ ) (D). The H37Rv WT-infected group is identical for A–D,  $n = 4$  mice per group.

not alter the outcome of infection (Fig. 3C). Additionally, overexpression of either *EsxG/H* or *EsxR/S* in the  $\Delta esxH$  strain restored virulence close to that of the WT strain (Fig. 3D).

A second model used a low-dose aerosol infection of immunocompetent C57BL/6 mice, where bacterial load in lung and spleen was measured at 4 and 11 wk postinfection. Whereas  $\Delta esxG$  and  $\Delta esxH$  exhibited low bacterial burdens, at or below the limit of detection, deletion of *rv3058c* in either of these mutants restored growth to WT levels in both lung and spleen (Fig. 4 A and B). In contrast, deletion of *rv3058c* in the WT background did not appreciably alter bacterial burden (Fig. 4 A and B). Therefore, in this model, as in the SCID model described above, the absence of *esxG* or *esxH* is required to reveal a phenotype for loss of *rv3058c*. Combined deletion of genes *esxR* and *esxS*, presumed to be under the regulation of Rv3058c, in a WT background also did not alter bacterial burdens in lung or spleen (Fig. 4 C and D). Bacterial numbers for the  $\Delta esxG/\Delta esxR/\Delta esxS$  and  $\Delta esxH/\Delta esxR/\Delta esxS$  combined deletion mutants were below the limit of detection in both lung and spleen at the two time points examined (Fig. 4 C and D). Because the parental  $\Delta esxG$  and  $\Delta esxH$  strains already exhibit substantial growth defects in this C57BL/6 low-dose aerosol model (Fig. 4 A and B) (22), it is difficult to assess whether the combined deletions of *esxR* and *esxS* contribute any additional attenuating impact. However, no apparent outgrowth of suppressors was observed for either of these combined deletion mutants.

**Extensive Amplification of the *esxRS* Locus in a Mouse Isolate.** In a separate experiment, following low-dose aerosol infection of C57BL/6 mice with  $\Delta esxGH::361-EV$ , which has the pMV361 EV integrated at the *attB* site and served as a control for the overexpression studies described above, a significant bacterial burden was detected at 1 mo postinfection. This result was surprising as the strain was expected to be growth-defective based on the *esxG* and *esxH* deletions. Genomic DNA prepared from

bacteria isolated from lungs was subjected to WGS, and for one of the three isolates ( $\Delta esxGH::361-EV$  M18, the  $\Delta esxGH::361-EV$  isolate recovered from mouse #18) (SI Appendix, Table S1), sequencing coverage across the *esxS-esxR* genes and immediate flanking regions was  $\sim 5,000$ -fold (Fig. 5A), as compared to only  $\sim 30$ -fold for neighboring loci. This finding was confirmed by qPCR analysis of *esxR* and *esxS* copy numbers in H37Rv WT, the parental  $\Delta esxGH::361-EV$  strain before passage through mice, and the three isolates recovered from mice (from mouse #17 [M17], #18 [M18], and #20 [M20]) (Fig. 5B). Again,  $\Delta esxGH::361-EV$  M18 displayed close to 100-fold greater copy numbers for *esxR* and *esxS* compared with the other strains (Fig. 5B). The genomic DNA was also examined by Southern blot, using a 537-bp probe containing *esxS-esxR* coding sequences (Dataset S2), which revealed the expected  $\sim 2,239$ -bp band for H37Rv WT (Fig. 5C). However, a tremendous increase in signal intensity was apparent for  $\Delta esxGH::361-EV$  M18, so much so that a prominent band was visible on the ethidium-bromide stained gel. Southern blotting confirmed that the band contained *esxS-esxR* sequences. Neither the  $\Delta esxGH::361-EV$  parent (before inoculation into animals) nor  $\Delta esxGH::361-EV$  M17 and M20 exhibited the exceptional increase in band intensity observed for the  $\Delta esxGH::361-EV$  M18 strain, although a doublet of two near-equal intensity bands was noted in the  $\Delta esxGH::361-EV$  parental strain. The basis for this doublet is not clear.

Illumina-based WGS using short reads, although well-suited for identifying SNPs and small insertions or deletions, has a limited ability to resolve large structural changes in the genome, such as gene duplications. Therefore, long-read Oxford Nanopore Technologies (ONT) MinION sequencing was employed to further characterize  $\Delta esxGH::361-EV$  M18. For comparison,  $\Delta esxGH::361-EV$  M20 was also sequenced as a representative *in vivo* isolate that lacked evidence of *esxRS* locus amplification. For  $\Delta esxGH::361-EV$  M18, a total of 2435 ONT raw reads were extracted for assembly. The longest read was over 171 kb, and the average sequence depth was 113-fold for the shorter contig

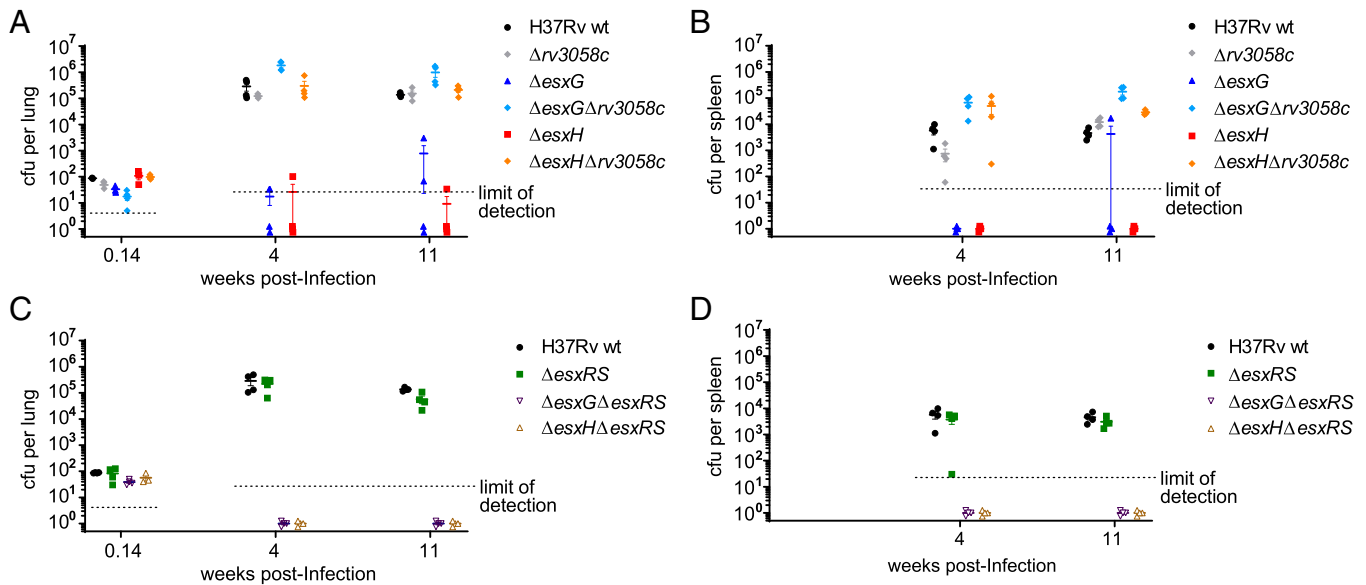


**Fig. 4.** Deletion of *rv3058c* is sufficient to restore in vivo growth of the  $\Delta$ *esxG* and  $\Delta$ *esxH* strains in aerosol-infected C57BL/6 mice. (A) Lung titers at the indicated times postinfection from mice infected via the aerosol route with H37Rv WT,  $\Delta$ *rv3058c*,  $\Delta$ *esxG*,  $\Delta$ *esxG*  $\Delta$ *rv3058c*,  $\Delta$ *esxH*, or  $\Delta$ *esxH*  $\Delta$ *rv3058c*. (B) Spleen titers for the mice in A. (C) Lung titers for mice infected by the aerosol route with H37Rv WT,  $\Delta$ *esxRS*,  $\Delta$ *esxG*  $\Delta$ *esxRS*, or  $\Delta$ *esxH*  $\Delta$ *esxRS*. (D) Spleen titers for the mice in C. For A–D, titers determined for individual mice are shown by symbols, while solid horizontal lines indicate means and error bars depict SEM. The limits of detection for the measurements are indicated by the dotted lines.  $n = 3$  to 4 mice per group per time point for A–D.

and 632-fold for the longer contig. The size of the stitched assembled genome was 4,583,652 bp.

The sequencing of  $\Delta$ *esxGH*::361-EV M18 revealed numerous tandem repeats, each 2,440 bp in length. Each repeat included the following gene sequence: *ppe48-ppe47-esxS-esxR-pe27A* (that is, *rv3022c-rv3021c-rv3020c-rv3019c-rv3018A*), with the nucleotide sequence of each repeat corresponding to that of the H37Rv parent strain (Fig. 6A). The longest repeat region captured was a single read greater than 132 kb in length, which consisted entirely of 54 tandem repeats. The sequencing also captured individual sequence “raw” reads consisting of 30 repeats adjacent to the chromosomal region downstream of *esxRS* and *pe27A* [i.e., genes *ppe46* (*rv3018c*)–*esxQ* (*rv3017c*)–*lppA* (*rv3016*)], and 38 repeats adjacent to the region upstream of *ppe48* [i.e., genes *trmU* (*rv3024c*)–*rv3023c-pe29* (*rv3022A*)] (Fig. 6A and B). These reads established the amplification as occurring at the native locus within the bacterial chromosome, rather than as repeats scattered throughout the chromosome or as an extrachromosomal event. Nanopore sequencing of the  $\Delta$ *esxGH*::361-EV M20 sample yielded a single large circular contig of ~4.4 Mb, which represents the complete genome, with no evidence of tandem repeats (SI Appendix, Fig. S4). However, a fully closed genome for  $\Delta$ *esxGH*::361-EV M18 (Fig. 6A) could not be assembled due to the tandem repeats, which exceeded the length of even the longest Nanopore reads. This suggests that there may be additional repeats not resolved by the Nanopore sequencing, a possibility supported by the estimated 100-fold greater copy number of *esxR* and *esxS* derived from qPCR.

To determine how the amplification impacts expression of the *esxRS* locus, we obtained total RNA from WT, the  $\Delta$ *esxGH* parent of the amplification strain and the amplification strain itself, after growth in 7H9 media lacking additional iron supplements. We then performed real-time qRT-PCR for *esxS* and a housekeeping gene, *sigA*, to which *esxS* expression was normalized. *EsxS* expression increased approximately ninefold over WT levels in the  $\Delta$ *esxGH* strain, possibly reflecting up-regulation due to iron starvation. Expression of *esxS* in  $\Delta$ *esxGH*::361-EV M18, in contrast, was up-regulated ~90-fold over its  $\Delta$ *esxGH* parent (Fig. 6C). This confirms that expression is up-regulated by the

amplification and the magnitude of the increase corresponds well to the number of repeats calculated by Nanopore sequencing and by qPCR of genomic DNA.

#### RNA Sequencing Provides Evidence that Derepression of *esxRS* Reverts the Iron-Starvation Phenotype of the $\Delta$ *esxG* Mutant.

To gain further insight into how derepression of *esxRS* can suppress  $\Delta$ *esxG* phenotypes, we examined the transcriptomes of *rv3058c* deletion mutants in the H37Rv and  $\Delta$ *esxG* backgrounds by RNA sequencing (RNA-seq). Following initial growth of all strains in 7H9 medium supplemented with 100  $\mu$ M hemin to facilitate optimal growth of the  $\Delta$ *esxG* mutants (22), bacteria were washed and inoculated into standard 7H9 medium without additional iron supplements, and triplicate samples were harvested for RNA isolation at day 3 (mid-log phase) and day 5 (late-log phase) postinoculation. Before harvesting, the OD<sub>600</sub> values for the strains were in similar ranges (~0.3 to 0.4 at day 3 and ~0.7 to 1.3 at day 5).

RNA-seq analysis comparing H37Rv  $\Delta$ *rv3058c* with H37Rv WT identified a total of seven genes that were up-regulated twofold or more in the  $\Delta$ *rv3058c* mutant at day 3 (SI Appendix, Table S5), consistent with Rv3058c acting as a repressor, similar to most other TetR-family members (31, 32). The sole down-regulated gene identified was *rv3058c*, which contained the targeted deletion; residual reads mapping to *rv3058c* were still detected in the mutant strain because the deletion spared the extreme 5' and 3' ends of the coding region (Dataset S3). Five of the seven up-regulated genes lie within the *esxRS* locus, including both *esxR* and *esxS*, and the *ppe* genes that flank them. Expression ratios of the genes in this region ranged from 2.28- to 3.50-fold greater for the mutant versus WT. The *rv3022A* gene at the 5' end of this presumed operon did not meet criteria for induction, as expression was only ~1.5-fold higher in the mutant than in WT (Dataset S3). The *rv0834c* gene (PE\_PGRS14) was also up-regulated (3.21-fold) at day 3 in  $\Delta$ *rv3058c*, as was *rv0989c* (*grcC2*; 4.04-fold) (SI Appendix, Table S5). Notably, both *rv0834c* and *rv3022A*, which is at the start of the *esxRS* locus (Fig. 2B), were identified by ChIP-seq analysis as having proximal, upstream intergenic Rv3058c

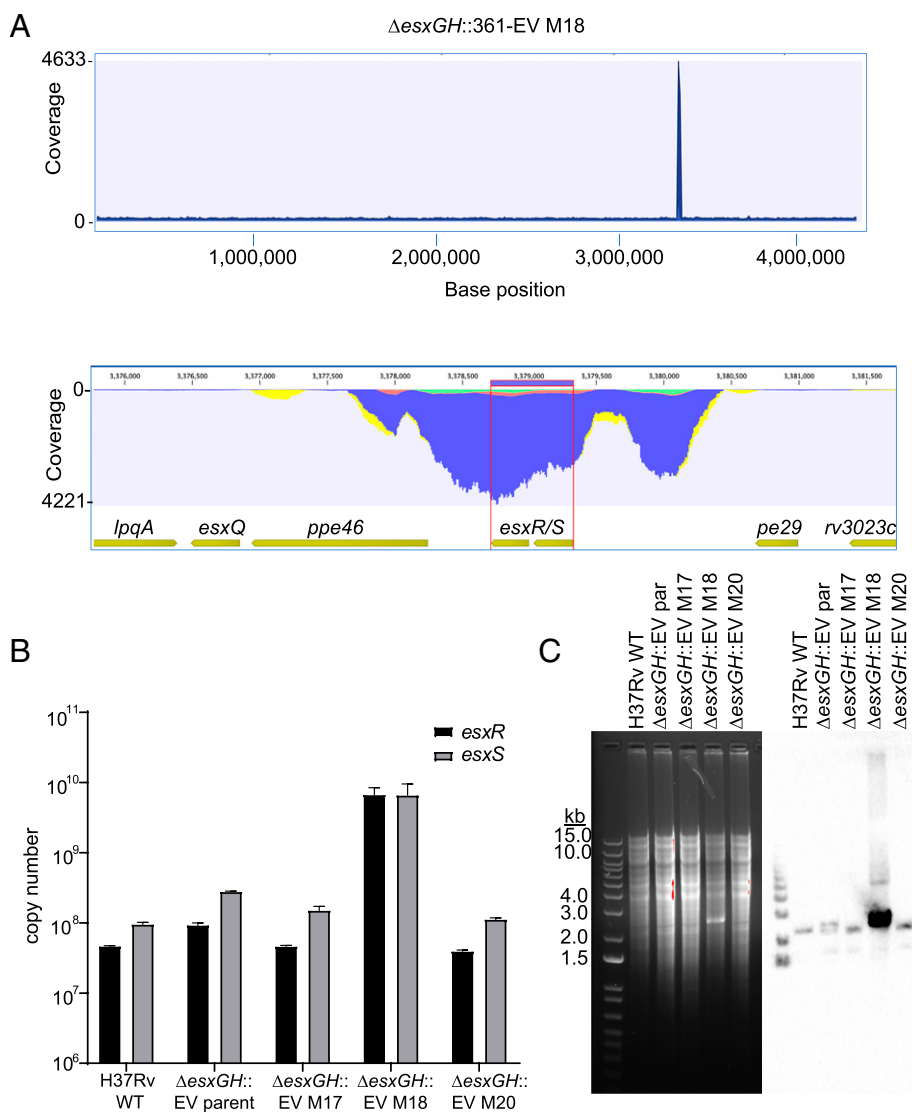


**Fig. 5.** Massive in vivo amplification of a portion of the *esxRS* locus in a  $\Delta esxGH$  strain. (A) Whole-genome Illumina sequencing read coverage (read length 150 bp) for strain H37Rv  $\Delta esxGH::361-EV M18$ . (Upper) Read coverage across the bacterial genome. (Lower) Zoom-in on an ~3-kb region that includes the *esxS*-*esxR* genes and flanking sequences, demonstrating that this region corresponds to the sharp spike in coverage seen in the Upper panel. (B) qPCR was performed in order to determine the *esxR* and *esxS* copy numbers in equivalent amounts of genomic DNA from H37Rv WT,  $\Delta esxGH::361-EV$  (the parental strain used to inoculate mice), and the three isolates recovered from mice #17, #18, and #20. The data represent the mean *esxR* and *esxS* copy numbers, determined in triplicate and calculated from standard curves. Error bars represent the SD. (C, Left) An ethidium bromide-stained agarose gel separating BamHI-digested genomic DNA from the indicated strains. (Right) The results of a Southern blot of the samples probed for *esxS*-*esxR*.

binding sites (35). Binding of purified recombinant Rv3058c at these sites by EMSA and reporter assays further confirmed these observations (SI Appendix, Fig. S2). These findings suggest that the enhanced expression observed in the deletion mutant is a direct result of the loss of repression by Rv3058c. Genes expressed at a higher level in  $\Delta rv3058c$  versus H37Rv at day 5 again included *rv0989c*, *rv0834c*, and *esxS* (Dataset S3). *EsxR* was just below the cutoff for fold-change in expression, at 1.965-fold higher in  $\Delta rv3058c$  than in WT.

When transcriptomes of  $\Delta esxG \Delta rv3058c$  were compared with those of  $\Delta esxG$ , the same pattern of gene-expression changes observed upon deletion of *rv3058c* in the H37Rv WT background was still apparent, although these were overlaid on a background of additional transcriptional changes, some metal-related, as described further below (Dataset S3). The seven genes up-regulated in the H37Rv  $\Delta rv3058c$  mutant at day 3 were also up-regulated approximately two- to fivefold in  $\Delta esxG \Delta rv3058c$  as compared with the  $\Delta esxG$  parent at this time point (SI Appendix, Table S5), and in fact were among the top 15 overexpressed genes when comparing the *rv3058c* deletion mutant to the parent. As noted above, five of these seven genes lie within the *esxRS* locus. *Rv0989c*, *rv0834c*, *esxS*, *esxR*, and *ppe46* were also up-regulated at day 5 in  $\Delta esxG \Delta rv3058c$  as compared with  $\Delta esxG$  (Dataset S3). The common changes in

both genetic backgrounds lend support to the transcriptional regulation of these genes by Rv3058c.

Additionally, several “metal-related” loci were down-regulated in  $\Delta esxG \Delta rv3058c$  as compared with  $\Delta esxG$  at both time points, including loci involved in synthesis of mycobactin siderophores and isonitrile lipopeptides (Dataset S3) (41–43). Also overexpressed in  $\Delta esxG$  as compared with the double mutant at day 3 were *rubA* (*rv3251c*) and *rubB* (*rv3250c*) (Dataset S3), genes encoding rubredoxins, small iron-sulfur proteins that act as electron carriers and play roles in oxidative stress responses (44); the rubredoxins are induced in *Mtb* under iron starvation (45). Together, these changes suggest at least a partial reversion of the iron starvation phenotype in the  $\Delta esxG \Delta rv3058c$  double mutant as compared with the  $\Delta esxG$  parent.

The global transcriptional impacts of *esxG* deletion and the extent to which these were modified by simultaneously deleting *rv3058c* were also assessed. A large number of differences were observed between the profiles of  $\Delta esxG$  and H37Rv WT, many reflecting a state of iron deprivation for the mutant (Dataset S3). To investigate this further, the top 50 differentially expressed genes between  $\Delta esxG$  and H37Rv WT at day 5 were identified, based on absolute  $\log_2$  fold-change, and the relative expression levels of this gene set in H37Rv WT,  $\Delta rv3058c$ ,  $\Delta esxG$ , and  $\Delta esxG \Delta rv3058c$  at days 3 and 5 were assessed (Fig. 7). The heat

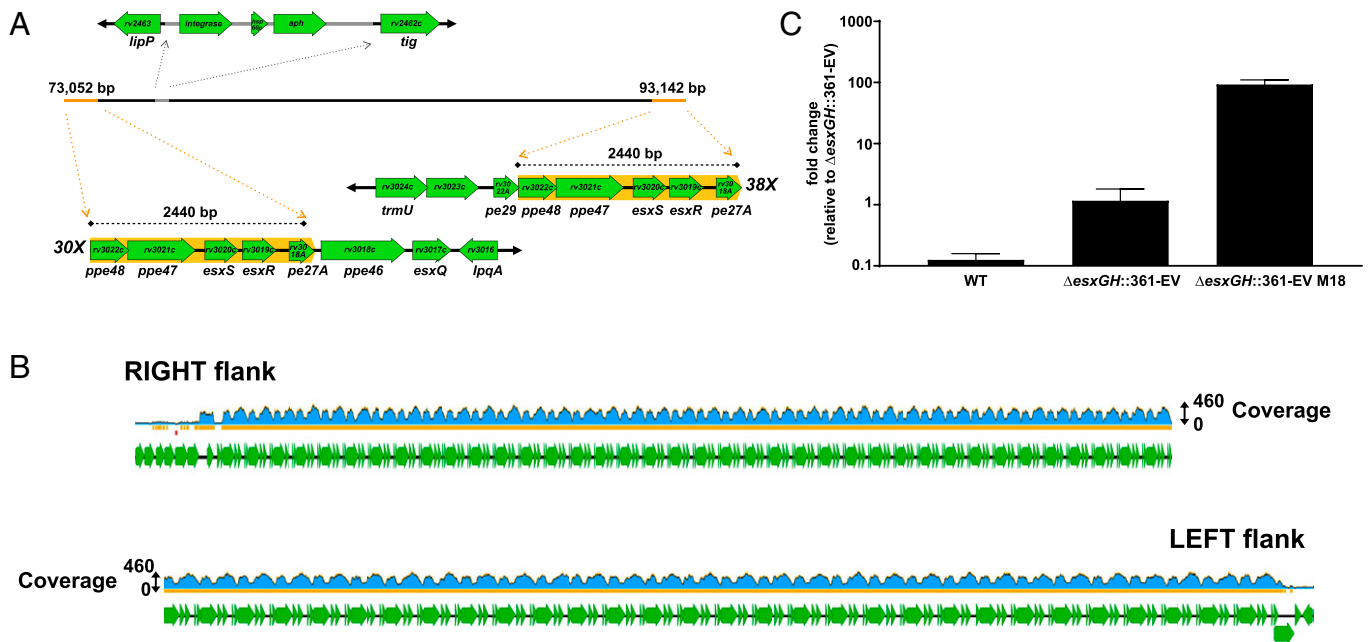


**Fig. 6.** Evidence for a massive in situ tandem amplification in  $\Delta esxGH::361\text{-EV}$  M18. (A) Nanopore sequencing of  $\Delta esxGH::361\text{-EV}$  M18 generated two contigs after Canu (v1.8) assembly, which were polished and stitched together to create a single linear contig on BioMatters Geneious R11 software by merging of overlapping sequences as described in *SI Appendix, SI Materials and Methods*. Annotation of the genome of  $\Delta esxGH::361\text{-EV}$  M18 with reference genome H37Rv (NC\_000962.3) revealed numerous tandem repeats of  $\sim 2,440$  bp in length at each end of the contig. The individual repeat units are highlighted with an orange background and flanking chromosomal sequences are also illustrated. As indicated, one end of the contig includes 30-fold repeats adjacent to neighboring genes *ppe46*, *esxQ*, and so forth, while the other end of the contig includes 38-fold repeats adjacent to the neighboring genes *pe29*, *rv3023c*, and so forth. A single copy of *integrase-hsp60* promoter-*aph* from the pMV361 vector inserted between *lipP* (*rv2463*) and *tig* (*rv2462c*) as revealed by Nanopore sequencing and annotation is shown in gray on the assembly. (B) Mapping of the Illumina reads to the constructed  $\Delta esxGH::361\text{-EV}$  M18 contig revealed a coverage as high as 460-fold along much of the tandem repeat region, versus 49-fold for the adjacent chromosomal loci on both the left and right flanks. This indicates that the number of repeats may actually be significantly larger than was captured by nanopore sequencing. (C) Expression of *esxS* in  $\Delta esxGH::361\text{-EV}$  M18 as compared with the H37Rv WT and parental ( $\Delta esxGH::361\text{-EV}$ ) strains was quantified by qRT-PCR. Data are represented as fold-change of RNA levels in the indicated strains as compared with the  $\Delta esxGH::361\text{-EV}$  strain. The data represent the mean and SD of three replicates.

map revealed a metal starvation signature for  $\Delta esxG$ , with up-regulation of numerous genes within the regulon of IdeR, as well as IdeR-independent, iron-repressed genes (14), and genes belonging to the Zur regulon (15). Similar transcriptional profiles were also observed upon down-regulation of the entire *esx-3* locus in a conditional mutant (19). As illustrated by the heat map (Fig. 7), although  $\Delta esxG \Delta rv3058c$  resembled  $\Delta esxG$  more closely than WT in terms of transcription patterns, it was still apparent that deletion of *rv3058c* in the  $\Delta esxG$  background partially reversed the iron-starvation signature, with the reversal being more apparent at day 5 than day 3 (Fig. 7). Principal component analysis also revealed the double mutant to lie between H37Rv WT and  $\Delta esxG$  (*SI Appendix, Fig. S5*).

## Discussion

The ESX-3 T7SS of *Mtb* plays critical roles in both iron acquisition and virulence (18–23). In the present study, we made the fortuitous and surprising discovery of suppressor mutations that rescued *Mtb esxG* and *esxH* mutants, enabling them to multiply and cause disease in infected mice. Analysis of the suppressor mutants from the diseased mice revealed that the *Mtb* mutations fell into two distinct classes, both associated with the *esxRS* locus. One of these involved the unprecedented, nearly 100-fold amplification of the *esxRS* locus. The second and most frequently identified class of mutations resulted in introduction of single amino acid changes in the DNA-binding domain of the putative TetR-family transcriptional regulator (TFTR) Rv3058c. These mutations appear to suppress *esxG* or *esxH* deletion phenotypes by up-regulating the *esxRS* locus, which encodes EsxR and EsxS. EsxQ is also present in the *esxRS* locus

and encodes a protein 65% identical to the N terminus of EsxH. Overall, the analyses performed further support the importance of ESX-3 in iron acquisition but also suggest that enhanced expression of the *esxRS* locus can compensate for the loss of the ESX-3 substrates EsxG and EsxH.

The first suppressor mutants recovered in vivo link the putative TFTR Rv3058c to the suppression of the  $\Delta esxG$  and  $\Delta esxH$  phenotypes and the regulation of *esxRS* expression. TFTRs possess N-terminal helix–turn–helix domains and C-terminal ligand-binding domains that regulate function. Although exceptions exist, in general, TFTRs act as repressors in the unliganded state (32, 46). Previous studies suggested a role for Rv3058c in regulation of the *esxRS* locus. Overexpression of *rv3058c* resulted in differential expression of 263 genes, including down-regulation of multiple genes within the *esxRS* locus (47). In this study, three independent nonsynonymous substitutions in *rv3058c* (H22D, R31H, and L33P) were identified in different suppressor strains. Based on the structures of TFTR family members (32, 33), these substitutions map to the putative N-terminal DNA-binding domain. A prior ChIP-seq study provided evidence for Rv3058c binding to the intergenic region between *rv3023c* and *pe29*, which is located upstream of the *esxRS* locus (35). Binding of recombinant purified WT Rv3058c to this site in EMSAs suggested that Rv3058c regulates at least some genes in this region, perhaps including *esxR* and *esxS*. WT and mutant Rv3058c were further assessed using a reporter gene assay that involved construction of a synthetic mammalian gene circuit to detect potential interaction of the Rv3058c protein with specific DNA sequences (37). An advantage of this approach, as opposed to testing in mycobacteria, is the expected absence of Rv3058c regulators and of competing

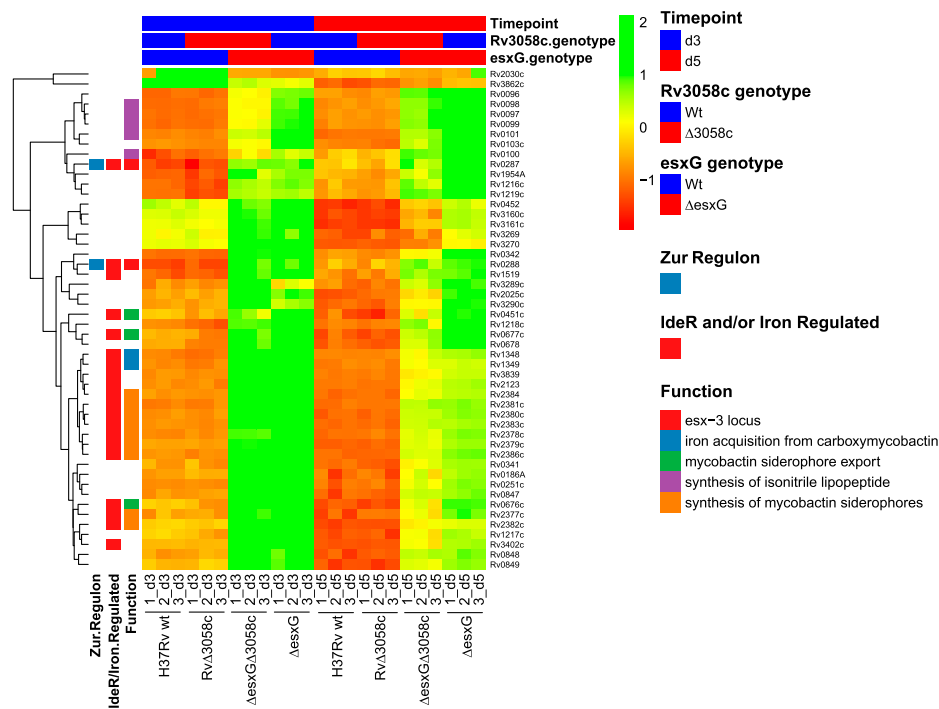


**Fig. 7.** Transcriptomic analysis using RNA-seq reveals a metal starvation signature for the  $\Delta$ esxG mutant grown in 7H9 medium, which is partially reversed by deleting *rv3058c*. The hierarchical clustering heat-map represents color-coded expression levels of the top 50 significant DEGs identified when comparing  $\Delta$ esxG with H37Rv WT at day 5 of growth in 7H9 medium, based on the  $\log_2$  fold-change values (false-discovery rate < 5%) as determined by RNA-seq analysis. Each row of the heat map represents a different gene as indicated to the right of the map and each column represents an individual sample as indicated below the map. The color and intensity of each cell are related to the normalized gene expression values, with green or red colors indicating up or down-regulation respectively and reordered according to the hierarchical clustering results. Several gene sets in functional categories relevant to this study are denoted by the colors in the legend on the right (Function). Genes that have previously been defined as being regulated by IdeR/iron or as belonging to the Zur regulon are indicated in the left-most columns. The groupings regarding time point, as well as *rv3058c* and *esxG* genotypes (WT or mutant) are indicated above the heat map.

mycobacterial transcription factors that might confound data interpretation. In this system, WT Rv3058c bound to the *rv3023c/pe29* intergenic region, as evidenced by activation of the reporter gene, whereas the R31H mutant was significantly less capable of activating this promoter or another Rv3058c target promoter, suggesting a defect in binding. Based on these data, we propose that Rv3058c negatively regulates expression of the *esxRS* locus by binding to the *rv3023c/pe29* intergenic region and that the point mutations disrupt binding, eliminating suppression of the locus. This interpretation is supported by the observation that the *rv3058c* deletion mutant phenocopied the suppressor mutants.

Overexpression of EsxR/S also phenocopied the *rv3058c* N-terminal point mutants and the deletion mutant with regard to complementing the iron supplementation requirements of the  $\Delta$ esxG/H strains. Using a constitutive promoter that would not be repressed by Rv3058c, this overexpression was sufficient to restore growth in the absence of iron supplementation but only when the ESX-3 secretory apparatus was intact. This suggests that EsxR and EsxS serve as substrates for the ESX-3 secretion system, much like EsxG and EsxH. Given the capacity of Rv3058c to bind upstream of the *esxRS* locus, we hypothesize that Rv3058c and the *esxRS* locus can function as an iron-acquisition regulon. Central to this model is the role of Rv3058c in regulating iron responses. When the entire *esx-3* region is intact, the function of the Rv3058c-EsxR/S regulon is presumably masked. However, impairment of ESX-3 function, as in the  $\Delta$ esxG and  $\Delta$ esxH strains, revealed the activity of the novel regulon. Consistent with the role of Rv3058c as a transcriptional repressor of the *esxRS* locus, RNA-seq revealed that seven differentially expressed genes (DEGs) were up-regulated in H37Rv  $\Delta$ rv3058c compared with H37Rv WT, including five genes from the *esxRS* locus. Comparison of  $\Delta$ esxG and H37Rv WT transcriptomes revealed that many DEGs reflective of an iron-starvation state were up-regulated in  $\Delta$ esxG, further supporting its importance in iron metabolism. The  $\Delta$ esxG profile was characterized by up-regulation of the IdeR regulon, of IdeR-independent, iron-repressed genes (14), and of genes in the Zur regulon (15). When comparing this set of genes across the mutants, it was found that  $\Delta$ esxG  $\Delta$ rv3058c resembled  $\Delta$ esxG more closely than it resembled

WT. Deletion of *rv3058c* in the  $\Delta$ esxG background nonetheless resulted in a partial reversion of the iron-starvation signature and also up-regulated the *esxRS* locus. These findings lend additional support to the hypotheses that Rv3058c is a negative regulator of *esxRS* locus and that up-regulation of EsxR/S, possibly with contributions of the flanking *pe-ppe* genes, allows iron acquisition.

It was previously demonstrated that deletions of the entire *esx-3* region or of *esxH* alone are highly attenuating in vivo (22). Here, it was discovered that deletion of *rv3058c* in the  $\Delta$ esxH or  $\Delta$ esxG background served to restore virulence in both a SCID mouse intravenous infection model and a C57BL/6 mouse aerosol model. Similarly, the  $\Delta$ esxH or  $\Delta$ esxG isolates encoding N-terminal substitution mutations in Rv3058c, originally recovered from C57BL/6 mice infected by aerosol, exhibited enhanced virulence when compared with the parental deletion strains in the SCID mouse model. Therefore, virulence phenotypes correlate with in vitro growth. No obvious phenotype was apparent for the *rv3058c* deletion in the H37Rv WT background, demonstrating again that the role of Rv3058c in regulation of the *esxRS* locus is revealed by the absence of EsxG/H function, at least in the mouse models examined. Moreover, because the  $\Delta$ esxG and  $\Delta$ esxH parental strains already exhibit substantial growth defects, any further attenuation due to *esxS-esxR* deletion could not be discerned in these strains. The presence in numerous *Mtb* strains of the *esxRS* locus and of a specific transcription factor that interacts with *cis*-acting regulatory sequences upstream of *esxRS* nonetheless suggest that this iron-acquisition regulon also plays a role for *Mtb* in a WT background.

It should be noted that several strains of *Mtb*, as well as sequenced isolates of *Mycobacterium microti*, lack *esxR* and *esxS*, while retaining portions of the flanking *pe-ppe* sequences and *esxQ* (48, 49). The loss of these sequences has been proposed to result from homologous recombination between the highly homologous *ppe* genes, *ppe46* (*rv3018c*) and *ppe47/48* (*rv3021c/rv3022c*), located upstream and downstream of *esxR* and *esxS* (48). The impact on growth and virulence of these polymorphisms within the *esxRS* locus is unknown. It is of interest that deletion of *pe18-pe26*, encoded within the *esx-5* locus

of *Mycobacterium canettii*, enhanced bacterial persistence in mice, demonstrating that loss of some *esx* region genes may facilitate pathogenesis (50). Related observations have been made for other mycobacteria as well. ESX-5-deficient *Mycobacterium marinum* displayed enhanced virulence in adult zebrafish (51). In the *Mtb* CDC1551 strain, deletion of the *ppe38* locus interfered with the secretion of numerous ESX-5 substrates and resulted in enhanced virulence in a mouse model; this deleted configuration at the *ppe38* locus is shared by *Mtb* strains from the Beijing lineage, which exhibit a hypervirulent phenotype (52, 53).

The most unexpected mechanism of suppression identified in this study was the massive, tandem amplification of a contiguous region of five genes from the *esxRS* locus: *ppe48-ppe47-esxS-esxR-pe27A*. This was identified in an in vivo isolate, suggesting that it restores virulence lost in  $\Delta$ *esxGH*. Based on several methods of analysis, this region is estimated to be present in as many as 100 tandem copies within the bacterial chromosome. The use of Nanopore-based sequencing to resolve the amplification in detail highlights the utility of very long-read approaches for identifying and characterizing such events. Recent WGS studies of clinical isolates of *Mtb* have uncovered impressive strain diversity (54–58), and WGS has documented an abundance of in vivo SNP differences that occur in the context of antibiotic exposure, host immune pressures, or at distinct anatomic sites within an infected host (56, 59, 60). Of note, the majority of these studies using WGS have excluded repetitive regions, such as the *pe/ppe* gene families and transposable/mobile elements in their analyses (55), due to ambiguities in alignment and assembly imposed by the mapping of short reads. This omission may have failed to capture the full breadth of genetic variation in *Mtb*. Although chromosomal duplications have been reported in mycobacteria (61–67), we are not aware of previous reports of such extensive gene amplification in this genus, as described in this study. Recently, plasmids have been identified that harbor ESX loci, and it has been hypothesized that duplication and divergence of these plasmid loci followed by migration to the chromosome may have contributed to the complex evolutionary history of the ESX regions (68–71). The data presented here suggest that duplication and amplification of *esx* and *pe/ppe* genes can occur within the chromosome, apart from plasmid sequences. It should be noted that the strain in which the amplification occurred harbored at the *attB* site an integrated pMV361 EV that encodes integrase. Whether integrase contributed to the magnitude of the amplification remains to be determined.

The extensive amplification of the *esxRS* locus may represent a genetic accordion. Genetic accordions involve the amplification of genes whose products inefficiently counteract a given selective pressure (72–74), such that increased gene copy numbers increase the dose of the needed product. Additionally, the increased copy number can allow for rare mutations to occur to one copy of the amplified gene, which can then efficiently counteract the selective pressure. This can result in reduction of the amplification because high dosage is no longer needed and because there is a cost associated with maintaining the amplification. Examples of accordion phenomena have been described in a variety of biological systems, including bacteria and DNA viruses, and provide a means by which pathogens can coevolve as the host develops novel antimicrobial strategies (73–78). Belikova et al. (79) observed that gene duplication and amplification occur frequently in the *Staphylococcus aureus* chromosome, concentrated in loci containing repetitive DNA elements that facilitate recombination; findings were consistent with an “accordion” model with high copy-number variants favored under selective conditions. An especially affected locus encoding “conserved staphylococcal antigens 1” (*csa1*) displayed amplification up to 10 copies in clinical isolates, while introduction of an antibiotic resistance cassette within the locus resulted

in amplifications up to 100- to 200-fold in the setting of antibiotic pressure (79). It will be of interest to determine if continued passage of the *esxRS* amplification strain under selective conditions in vitro or in vivo might yield strains with mutations that then allow contraction of the amplification.

Gene duplication, amplification, and divergence have been hypothesized to represent a major mechanism underlying the emergence of genes with novel functions (72, 80). Such phenomena appear to have played a role in the evolution of the PE/PPE families of proteins, as well as the emergence of the five ESX loci. In addition to the *esx* genes encoded within the ESX-1 to -5 regions (two per locus), at least 13 *esx* paralogs outside of these have been identified in H37Rv based on sequence homology, with an additional *esx* pair present in some isolates (6, 53, 81–84). Although most Esx proteins encoded apart from secretion systems lack well-defined functions, ESX-5 paralogs encoded within the ESX5a locus of *Mtb* and *M. marinum* facilitate the secretion of a subset of ESX-5 substrates (85). The EsxE-EsxF proteins, which lack homology with conserved ESX loci, mediate secretion of the tuberculosis necrotizing toxin (86). Similar to the present study, functional substitution by Esx paralogs has been reported in *M. marinum*, which possesses several duplications of *esxB* and *esxA*, which can functionally complement ESX-1-mediated activities (87).

The present study attributes function to the *esxRS* locus, which contains *esxR*, *esxS*, and *esxQ*, and is related to ESX-3. Specifically, we provide conclusive evidence that EsxR/S can assume the function of ESX-3 substrates in iron acquisition and virulence. Whether other functions of ESX-3 are also carried out by the *esxRS* region remains to be determined. For example, EsxH is an immunodominant antigen in the murine tuberculosis model where it stimulates potent T cell responses and may function as a decoy antigen; EsxH is also a target of human T cell responses and interacts with the host cell ESCRT machinery to modulate antigen presentation (24, 25, 88–92). Furthermore, a number of unique T cell epitopes have been identified in EsxR (89, 93); it remains to be determined whether EsxR has immunological functions similar to those reported for EsxH and whether such activities are relevant to the suppressor function of the *esxRS* locus.

In summary, our data illustrate how *Mtb* can take advantage of one apparent product of gene duplication in the *esxRS* locus to overcome, by at least two distinct genetic mechanisms, the severe attenuation conferred by mutations in EsxG and EsxH. The findings highlight the remarkable genetic plasticity that allows *Mtb* to overcome the loss of a key nutrient acquisition pathway. Beyond this, our work reveals the possibility that these genes can be amplified to high numbers using an accordion mechanism of amplification. Interestingly, despite its capabilities, PacBio sequencing has heretofore not revealed such amplifications. Our work clearly establishes that *Mtb* can accommodate such amplifications and future work will be required to elucidate the mechanisms.

## Materials and Methods

**Bacterial Strains and Culture Conditions.** Mycobacterial strains were grown in Middlebrook 7H9 medium (Difco) supplemented with 10% (vol/vol) OADC enrichment (0.5 g oleic acid, 50 g albumin, 20 g dextrose, 0.04 g catalase, 8.5 g sodium chloride in 1 L water), 0.2% (vol/vol) glycerol, and 0.05% (vol/vol) tyloxapol (Sigma). Supplemented media for culturing strains with mutations within the *esx-3* locus also included 100  $\mu$ M hemin (Sigma). Antibiotic selection media contained 50 to 75  $\mu$ g/mL hygromycin B (Gold Biotechnology) or 25  $\mu$ g/mL kanamycin as required. For cloning in *E. coli*, hygromycin was used at 150  $\mu$ g/mL and kanamycin at 25 to 40  $\mu$ g/mL.

**Bacterial Strain Construction.** Plasmids and mycobacterial strains are detailed in *SI Appendix, Tables S3 and S4*, respectively. H37Rv was the parental *Mtb* strain for all mutants used and generated in this study. The construction and unmarking of  $\Delta$ *esxG*,  $\Delta$ *esxH*,  $\Delta$ *esxGH*, and  $\Delta$ *esx-3* strains and the

complementation of the unmarked  $\Delta\text{esxG}$  strain have been described previously (22). The introduction of *rv3058c* deletions into H37Rv,  $\Delta\text{esxG}$ ,  $\Delta\text{esxH}$ , and  $\Delta\text{esx-3}$ , and of *esxS-esxR* deletions into H37Rv,  $\Delta\text{esxG}$ , and  $\Delta\text{esxH}$  using specialized transduction (94, 95) is described in *SI Appendix, SI Materials and Methods*, as are the unmarking (removal of the *sacB*-hygromycin cassette) and complementation of the indicated strains.

**Solid Media Growth Experiments.** Bacterial cultures grown to log phase were washed in PBS containing 0.05% tyloxapol (PBS-T), resuspended in PBS-T, and adjusted to equivalent OD<sub>600</sub> values. Following serial dilution, equivalent inocula were plated in parallel onto 7H10 base medium containing 10% OADC and 0.5% glycerol, and either lacking or containing 200 ng/mL mycobactin J. Plates were incubated for ~3 to 6 wk at 37 °C.

**WGS.** Genomic DNA was extracted from H37Rv WT and mutant strains by the hexadecyltrimethylammonium bromide-lysozyme method using established protocols (96) and WGS was conducted using Illumina and Nanopore MinION, as described in *SI Appendix, SI Materials and Methods*.

**Protein Expression and Purification.** The expression and purification of Rv3058c WT, R31H, and H22D/R31H/L33P mutants is described in *SI Appendix, SI Materials and Methods*.

**SEAP Reporter Assay.** Construction of transcriptional regulator-expressing plasmids encoding *Rv3058c*-VP16 chimeras and of plasmids containing the promoter regions from *rv0834c* and *pe29* designed to assess the DNA-binding capacity of the chimeras is described in *SI Appendix, SI Materials and Methods*; plasmids used in this study are listed in *SI Appendix, Table S3*. The *SI Appendix, SI Materials and Methods* also provides details of the transfections and SEAP assays.

**EMSA.** EMSA were performed to assess the DNA binding capacity of Rv3058c WT, using the ~200-bp sequences upstream of *rv0834c* and *pe29* as probes (Dataset S2). The EMSA reactions were prepared using the Invitrogen Molecular Probes SYBR SYPRO Electrophoretic Mobility-Shift Assay (EMSA) Kit (Thermo Fisher Scientific) according to the manufacturer's instructions. Details of probe preparation, binding reaction composition, and imaging are provided in *SI Appendix, SI Materials and Methods*.

**qPCR of *esxR* and *esxS* in Amplification Strain.** An absolute quantitative real-time PCR assay using the Evagreen Dye and qPCR Master Mix kit (Biotium) was performed to determine *esxR* and *esxS* gene copy numbers in selected strains, as detailed in *SI Appendix, SI Materials and Methods*.

**Southern Blot of *esxR5* Amplification Strain.** Genomic DNA was extracted using established protocols (96) from H37Rv WT,  $\Delta\text{esxGH}$  transformed with pMV361 EV ( $\Delta\text{esxGH}::361\text{-EV}$ ), and three isolates of  $\Delta\text{esxGH}::361\text{-EV}$  recovered from mice and Southern blotting performed as described in *SI Appendix, SI Materials and Methods*.

**qRT-PCR Analysis of *esxS* Expression.** RNA was extracted from the relevant strains and subjected to qRT-PCR; relative *esxS* gene expression levels were determined using the  $2^{-\Delta\Delta C_t}$  method, with *sigA* serving as the housekeeping control gene. Further details are provided in *SI Appendix, SI Materials and Methods*.

**Transcriptome Analysis.** Procedures for extraction of RNA from H37Rv WT, H37Rv  $\Delta\text{rv3058c}$ ,  $\Delta\text{esxG}$ , and  $\Delta\text{esxG } \Delta\text{rv3058c}$ , for RNA-seq library preparation and sequencing and for bioinformatic analyses are provided in *SI Appendix, SI Materials and Methods*.

**Mouse infections.** Mouse studies were performed in accordance with National Institutes of Health guidelines, and all work was approved by the Albert Einstein College of Medicine Institutional Animal Care and Use Committee. Details of aerosol and intravenous infection protocols are provided in *SI Appendix, SI Materials and Methods*.

**Data Availability.** The raw reads reported in this paper have been deposited in the National Center for Biotechnology Information's Sequence Read Archive (BioProject PRJNA784324) (97). All other study data are included in the article and/or supporting information.

**ACKNOWLEDGMENTS.** We thank Annie Dai, John Kim, Mei Chen, Laura Cole, and Jack Fischer for expert technical assistance; and Susan Howard for critical reading of the manuscript. This work was supported by NIH Grants U19AI109945 (to C.F.B.), P01AI120943 (to C.F.B., D.W.L., and G.K.A.), A1137344 (to J.C.), and A1026170 (to W.R.J.); Department of Defense Grant W81XWH2010099 (to J.M.T.); and funds to J.M.T. and C.F.B. from Georgia State University.

- World Health Organization, *Global Tuberculosis Report 2016* (World Health Organization, Geneva, 2016).
- J. Rybniker *et al.*, Anticytolytic screen identifies inhibitors of mycobacterial virulence protein secretion. *Cell Host Microbe* **16**, 538–548 (2014).
- M. I. Gröschel, F. Sayes, R. Simeone, L. Majlessi, R. Brosch, ESX secretion systems: Mycobacterial evolution to counter host immunity. *Nat. Rev. Microbiol.* **14**, 677–691 (2016).
- K. A. Sweeney *et al.*, A recombinant *Mycobacterium smegmatis* induces potent bactericidal immunity against *Mycobacterium tuberculosis*. *Nat. Med.* **17**, 1261–1268 (2011).
- S. Tiwari *et al.*, BCG-prime and boost with *Esx-5* secretion system deletion mutant leads to better protection against clinical strains of *Mycobacterium tuberculosis*. *Vaccine* **38**, 7156–7165 (2020).
- W. Bitter *et al.*, Systematic genetic nomenclature for type VII secretion systems. *PLoS Pathog.* **5**, e1000507 (2009).
- M. J. Pallen, The ESAT-6/WXG100 superfamily—And a new Gram-positive secretion system? *Trends Microbiol.* **10**, 209–212 (2002).
- A. M. Abdallah *et al.*, Type VII secretion—Mycobacteria show the way. *Nat. Rev. Microbiol.* **5**, 883–891 (2007).
- P. A. Champion, J. S. Cox, Protein secretion systems in mycobacteria. *Cell. Microbiol.* **9**, 1376–1384 (2007).
- S. A. Stanley, J. S. Cox, Host-pathogen interactions during *Mycobacterium tuberculosis* infections. *Curr. Top. Microbiol. Immunol.* **374**, 211–241 (2013).
- R. Simeone, D. Bottai, R. Brosch, ESX/type VII secretion systems and their role in host-pathogen interaction. *Curr. Opin. Microbiol.* **12**, 4–10 (2009).
- E. J. Stoop, W. Bitter, A. M. van der Sar, Tubercle bacilli rely on a type VII army for pathogenicity. *Trends Microbiol.* **20**, 477–484 (2012).
- D. Bottai, M. I. Gröschel, R. Brosch, Type VII secretion systems in Gram-positive bacteria. *Curr. Top. Microbiol. Immunol.* **404**, 235–265 (2017).
- G. M. Rodriguez, M. I. Voskuil, B. Gold, G. K. Schoolnik, I. Smith, *ideR*, An essential gene in *Mycobacterium tuberculosis*: Role of *IdeR* in iron-dependent gene expression, iron metabolism, and oxidative stress response. *Infect. Immun.* **70**, 3371–3381 (2002).
- A. Maciagi *et al.*, Global analysis of the *Mycobacterium tuberculosis* Zur (FurB) regulon. *J. Bacteriol.* **189**, 730–740 (2007).
- R. Pandey *et al.*, MntR(Rv2788): A transcriptional regulator that controls manganese homeostasis in *Mycobacterium tuberculosis*. *Mol. Microbiol.* **98**, 1168–1183 (2015).
- X. Li *et al.*, A novel stress-inducible CmtR-ESX3-Zn<sup>2+</sup> regulatory pathway essential for survival of *Mycobacterium bovis* under oxidative stress. *J. Biol. Chem.* **295**, 17083–17099 (2020).
- A. Serafini, F. Boldrin, G. Palù, R. Manganelli, Characterization of a *Mycobacterium tuberculosis* ESX-3 conditional mutant: Essentiality and rescue by iron and zinc. *J. Bacteriol.* **191**, 6340–6344 (2009).
- A. Serafini, D. Pisu, G. Palù, G. M. Rodriguez, R. Manganelli, The ESX-3 secretion system is necessary for iron and zinc homeostasis in *Mycobacterium tuberculosis*. *PLoS One* **8**, e78351 (2013).
- M. S. Siegrist *et al.*, Mycobacterial Esx-3 requires multiple components for iron acquisition. *MBio* **5**, e01073-14 (2014).
- M. S. Siegrist *et al.*, Mycobacterial Esx-3 is required for mycobactin-mediated iron acquisition. *Proc. Natl. Acad. Sci. U.S.A.* **106**, 18792–18797 (2009).
- J. M. Tufariello *et al.*, Separable roles for *Mycobacterium tuberculosis* ESX-3 effectors in iron acquisition and virulence. *Proc. Natl. Acad. Sci. U.S.A.* **113**, E348–E357 (2016).
- L. Zhang *et al.*, Comprehensive analysis of iron utilization by *Mycobacterium tuberculosis*. *PLoS Pathog.* **16**, e1008337 (2020).
- C. Portal-Celhay *et al.*, *Mycobacterium tuberculosis* EsxH inhibits ESCRT-dependent CD4<sup>+</sup> T-cell activation. *Nat. Microbiol.* **2**, 16232 (2016).
- J. D. Yang *et al.*, *Mycobacterium tuberculosis*-specific CD4<sup>+</sup> and CD8<sup>+</sup> T cells differ in their capacity to recognize infected macrophages. *PLoS Pathog.* **14**, e1007060 (2018).
- G. L. Beamer *et al.*, Interleukin-10 promotes *Mycobacterium tuberculosis* disease progression in CBA/J mice. *J. Immunol.* **181**, 5545–5550 (2008).
- C. Keller *et al.*, Genetically determined susceptibility to tuberculosis in mice causally involves accelerated and enhanced recruitment of granulocytes. *Infect. Immun.* **74**, 4295–4309 (2006).
- E. Medina, R. J. North, Evidence inconsistent with a role for the *Bcg* gene (*Nramp1*) in resistance of mice to infection with virulent *Mycobacterium tuberculosis*. *J. Exp. Med.* **183**, 1045–1051 (1996).
- E. Medina, R. J. North, Resistance ranking of some common inbred mouse strains to *Mycobacterium tuberculosis* and relationship to major histocompatibility complex haplotype and *Nramp1* genotype. *Immunology* **93**, 270–274 (1998).
- J. Turner *et al.*, Immunological basis for reactivation of tuberculosis in mice. *Infect. Immun.* **69**, 3264–3270 (2001).
- R. J. Balhana, A. Singla, M. H. Sikder, M. Withers, S. L. Kendall, Global analyses of TetR family transcriptional regulators in mycobacteria indicates conservation across species and diversity in regulated functions. *BMC Genomics* **16**, 479 (2015).
- L. Cuthbertson, J. R. Nodwell, The TetR family of regulators. *Microbiol. Mol. Biol. Rev.* **77**, 440–475 (2013).

33. J. L. Ramos *et al.*, The TetR family of transcriptional repressors. *Microbiol. Mol. Biol. Rev.* **69**, 326–356 (2005).
34. J. E. Galagan *et al.*, TB database 2010: Overview and update. *Tuberculosis (Edinb.)* **90**, 225–235 (2010).
35. K. J. Minch *et al.*, The DNA-binding network of *Mycobacterium tuberculosis*. *Nat. Commun.* **6**, 5829 (2015).
36. T. B. Reddy *et al.*, TB database: An integrated platform for tuberculosis research. *Nucleic Acids Res.* **37**, D499–D508 (2009).
37. N. Blondiaux *et al.*, Reversion of antibiotic resistance in *Mycobacterium tuberculosis* by spiroisoxazoline SMART-420. *Science* **355**, 1206–1211 (2017).
38. P. O’Gaora, “Expression of genes in mycobacteria” in *Mycobacteria Protocols*, T. Parish, N. G. Stoker, Eds. (Humana Press, Totawa, NJ, 1998), pp. 261–273.
39. M. A. Arbing *et al.*, The crystal structure of the *Mycobacterium tuberculosis* Rv3019c-Rv3020c ESX complex reveals a domain-swapped heterotetramer. *Protein Sci.* **19**, 1692–1703 (2010).
40. D. Ilghari *et al.*, Solution structure of the *Mycobacterium tuberculosis* EsxG:EsxH complex: Functional implications and comparisons with other *M. tuberculosis* Esx family complexes. *J. Biol. Chem.* **286**, 29993–30002 (2011).
41. N. C. Harris *et al.*, Biosynthesis of isonitrile lipopeptides by conserved nonribosomal peptide synthetase gene clusters in Actinobacteria. *Proc. Natl. Acad. Sci. U.S.A.* **114**, 7025–7030 (2017).
42. R. Krithika *et al.*, A genetic locus required for iron acquisition in *Mycobacterium tuberculosis*. *Proc. Natl. Acad. Sci. U.S.A.* **103**, 2069–2074 (2006).
43. L. E. Quadri, J. Sello, T. A. Keating, P. H. Weinreb, C. T. Walsh Identification of a *Mycobacterium tuberculosis* gene cluster encoding the biosynthetic enzymes for assembly of the virulence-conferring siderophore mycobactin. *Chem. Biol.* **5**, 631–645 (1998).
44. T. Sushko *et al.*, A new twist of rubredoxin function in *M. tuberculosis*. *Bioorg. Chem.* **109**, 104721 (2021).
45. K. Kurthkoti *et al.*, The capacity of *Mycobacterium tuberculosis* to survive iron starvation might enable it to persist in iron-deprived microenvironments of human granulomas. *mBio* **8**, e01092-17 (2017).
46. P. Nguyen Le Minh *et al.*, Ligand binding specificity of RutR, a member of the TetR family of transcription regulators in *Escherichia coli*. *FEBS Open Bio* **5**, 76–84 (2015).
47. T. R. Rustad *et al.*, Mapping and manipulating the *Mycobacterium tuberculosis* transcriptome using a transcription factor overexpression-derived regulatory network. *Genome Biol.* **15**, 502 (2014).
48. M. Marmiesse *et al.*, Macro-array and bioinformatic analyses reveal mycobacterial ‘core’ genes, variation in the ESAT-6 gene family and new phylogenetic markers for the *Mycobacterium tuberculosis* complex. *Microbiology (Reading)* **150**, 483–496 (2004).
49. M. Orgeur *et al.*, Pathogenomic analyses of *Mycobacterium microti*, an ESX-1-deleted member of the *Mycobacterium tuberculosis* complex causing disease in various hosts. *Microb. Genom.* **7**, 000505 (2021).
50. A. C. Allen *et al.*, Parallel in vivo experimental evolution reveals that increased stress resistance was key for the emergence of persistent tuberculosis bacilli. *Nat. Microbiol.* **6**, 1082–1093 (2021).
51. E. M. Weerdenburg *et al.*, ESX-5-deficient *Mycobacterium marinum* is hypervirulent in adult zebrafish. *Cell. Microbiol.* **14**, 728–739 (2012).
52. L. S. Ates *et al.*, Mutations in ppe38 block PE<sub>3</sub>GRS secretion and increase virulence of *Mycobacterium tuberculosis*. *Nat. Microbiol.* **3**, 181–188 (2018).
53. C. R. McEvoy, P. D. van Helden, R. M. Warren, N. C. Gey van Pittius, Evidence for a rapid rate of molecular evolution at the hypervariable and immunogenic *Mycobacterium tuberculosis* PPE38 gene region. *BMC Evol. Biol.* **9**, 237 (2009).
54. A. Van Rie, C. Meehan, The devil is in the diversity: Exploring within-person evolution of *Mycobacterium tuberculosis*. *EBioMedicine* **55**, 102758 (2020).
55. S. D. Ley, M. de Vos, A. Van Rie, R. M. Warren, Deciphering within-host microevolution of *Mycobacterium tuberculosis* through whole-genome sequencing: The phenotypic impact and way forward. *Microbiol. Mol. Biol. Rev.* **83**, e00062-18 (2019).
56. C. Nimmo *et al.*, Dynamics of within-host *Mycobacterium tuberculosis* diversity and heteroresistance during treatment. *EBioMedicine* **55**, 102747 (2020).
57. C. Ford *et al.*, *Mycobacterium tuberculosis*—Heterogeneity revealed through whole genome sequencing. *Tuberculosis (Edinb.)* **92**, 194–201 (2012).
58. S. J. Modlin *et al.*, Drivers and sites of diversity in the DNA adenine methylomes of 93 *Mycobacterium tuberculosis* complex clinical isolates. *eLife* **9**, e58542 (2020).
59. T. D. Lieberman *et al.*, Genomic diversity in autopsy samples reveals within-host dissemination of HIV-associated *Mycobacterium tuberculosis*. *Nat. Med.* **22**, 1470–1474 (2016).
60. Q. Liu *et al.*, *Mycobacterium tuberculosis* clinical isolates carry mutational signatures of host immune environments. *Sci. Adv.* **6**, eaba4901 (2020).
61. R. Brosch *et al.*, Genome plasticity of BCG and impact on vaccine efficacy. *Proc. Natl. Acad. Sci. U.S.A.* **104**, 5596–5601 (2007).
62. P. Domenech, G. S. Kolly, L. Leon-Solis, A. Fallow, M. B. Reed, Massive gene duplication event among clinical isolates of the *Mycobacterium tuberculosis* W/Beijing family. *J. Bacteriol.* **192**, 4562–4570 (2010).
63. A. Galamba *et al.*, Disruption of *adhC* reveals a large duplication in the *Mycobacterium smegmatis* mc(2)155 genome. *Microbiology (Reading)* **147**, 3281–3294 (2001).
64. A. S. Leung *et al.*, Novel genome polymorphisms in BCG vaccine strains and impact on efficacy. *BMC Genomics* **9**, 413 (2008).
65. X. M. Wang *et al.*, IS1096-mediated DNA rearrangements play a key role in genome evolution of *Mycobacterium smegmatis*. *Tuberculosis (Edinb.)* **88**, 399–409 (2008).
66. B. Weiner *et al.*, Independent large scale duplications in multiple *M. tuberculosis* lineages overlapping the same genomic region. *PLoS One* **7**, e26038 (2012).
67. R. Brosch *et al.*, Comparative genomics uncovers large tandem chromosomal duplications in *Mycobacterium bovis* BCG Pasteur. *Yeast* **17**, 111–123 (2000).
68. R. Ummels *et al.*, Identification of a novel conjugative plasmid in mycobacteria that requires both type IV and type VII secretion. *MBio* **5**, e01744-14 (2014).
69. E. Dumas *et al.*, Mycobacterial pan-genome analysis suggests important role of plasmids in the radiation of type VII secretion systems. *Genome Biol. Evol.* **8**, 387–402 (2016).
70. M. Newton-Foot, R. M. Warren, S. L. Sampson, P. D. van Helden, N. C. Gey van Pittius, The plasmid-mediated evolution of the mycobacterial ESX (type VII) secretion systems. *BMC Evol. Biol.* **16**, 62 (2016).
71. T. D. Mortimer, A. M. Weber, C. S. Pepperell, Evolutionary thrift: Mycobacteria repurpose plasmid diversity during adaptation of type VII secretion systems. *Genome Biol. Evol.* **9**, 398–413 (2017).
72. U. Bergthorsson, D. I. Andersson, J. R. Roth, Ohno’s dilemma: Evolution of new genes under continuous selection. *Proc. Natl. Acad. Sci. U.S.A.* **104**, 17004–17009 (2007).
73. N. C. Elde *et al.*, Poxviruses deploy genomic accordions to adapt rapidly against host antiviral defenses. *Cell* **150**, 831–841 (2012).
74. J. R. Roth, D. I. Andersson, Poxvirus use a “gene accordion” to tune out host defenses. *Cell* **150**, 671–672 (2012).
75. D. I. Andersson, E. S. Slechts, J. R. Roth, Evidence that gene amplification underlies adaptive mutability of the bacterial lac operon. *Science* **282**, 1133–1135 (1998).
76. E. S. Slechts *et al.*, Adaptive mutation: General mutagenesis is not a programmed response to stress but results from rare coamplification of *dinB* with *lac*. *Proc. Natl. Acad. Sci. U.S.A.* **100**, 12847–12852 (2003).
77. M. Pránting, D. I. Andersson, Escape from growth restriction in small colony variants of *Salmonella typhimurium* by gene amplification and mutation. *Mol. Microbiol.* **79**, 305–315 (2011).
78. S. D. Copley, Toward a systems biology perspective on enzyme evolution. *J. Biol. Chem.* **287**, 3–10 (2012).
79. D. Belikova, A. Jochim, J. Power, M. T. G. Holden, S. Heilbronner, “Gene accordions” cause genotypic and phenotypic heterogeneity in clonal populations of *Staphylococcus aureus*. *Nat. Commun.* **11**, 3526 (2020).
80. M. P. Francino, An adaptive radiation model for the origin of new gene functions. *Nat. Genet.* **37**, 573–577 (2005).
81. S. T. Cole *et al.*, Deciphering the biology of *Mycobacterium tuberculosis* from the complete genome sequence. *Nature* **393**, 537–544 (1998).
82. N. C. Gey Van Pittius *et al.*, The ESAT-6 gene cluster of *Mycobacterium tuberculosis* and other high G+C Gram-positive bacteria. *Genome Biol.* **2**, RESEARCH0044 (2001).
83. F. Tekaija *et al.*, Analysis of the proteome of *Mycobacterium tuberculosis* in silico. *Tuber. Lung Dis.* **79**, 329–342 (1999).
84. S. Uplekar, B. Heym, V. Friocourt, J. Rougemont, S. T. Cole, Comparative genomics of Esx genes from clinical isolates of *Mycobacterium tuberculosis* provides evidence for gene conversion and epitope variation. *Infect. Immun.* **79**, 4042–4049 (2011).
85. S. Shah, J. R. Cannon, C. Fenselau, V. Briken, A duplicated ESAT-6 region of ESX-5 is involved in protein export and virulence of mycobacteria. *Infect. Immun.* **83**, 4349–4361 (2015).
86. U. Tak, T. Dokland, M. Niederweis, Pore-forming Esx proteins mediate toxin secretion by *Mycobacterium tuberculosis*. *Nat. Commun.* **12**, 394 (2021).
87. R. E. Bosserman, C. R. Thompson, K. R. Nicholson, P. A. Champion, Esx paralogs are functionally equivalent to ESX-1 proteins but are dispensable for virulence in *Mycobacterium marinum*. *J. Bacteriol.* **200**, e00726-17 (2018).
88. C. Nunes-Alves *et al.*, Human and murine clonal CD8+ T cell expansions arise during tuberculosis because of TCR selection. *PLoS Pathog.* **11**, e1004849 (2015).
89. R. L. Skjot *et al.*, Epitope mapping of the immunodominant antigen TB10.4 and the two homologous proteins TB10.3 and TB12.9, which constitute a subfamily of the *esat-6* gene family. *Infect. Immun.* **70**, 5446–5453 (2002).
90. R. L. Skjot *et al.*, Comparative evaluation of low-molecular-mass proteins from *Mycobacterium tuberculosis* identifies members of the ESAT-6 family as immunodominant T-cell antigens. *Infect. Immun.* **68**, 214–220 (2000).
91. D. A. Lewinsohn *et al.*, Comprehensive definition of human immunodominant CD8 antigens in tuberculosis. *NPI Vaccines* **2**, 8 (2017).
92. R. Sutuwisesak *et al.*, A natural polymorphism of *Mycobacterium tuberculosis* in the *esxH* gene disrupts immunodomination by the TB10.4-specific CD8 T cell response. *PLoS Pathog.* **16**, e1009000 (2020).
93. T. Lindenstrom, C. Aagaard, D. Christensen, E. M. Agger, P. Andersen, High-frequency vaccine-induced CD8+ T cells specific for an epitope naturally processed during infection with *Mycobacterium tuberculosis* do not confer protection. *Eur. J. Immunol.* **44**, 1699–1709 (2014).
94. S. Bardarov *et al.*, Specialized transduction: An efficient method for generating marked and unmarked targeted gene disruptions in *Mycobacterium tuberculosis*, *M. bovis* BCG and *M. smegmatis*. *Microbiology (Reading)* **148**, 3007–3017 (2002).
95. P. Jain *et al.*, Specialized transduction designed for precise high-throughput unmarked deletions in *Mycobacterium tuberculosis*. *MBio* **5**, e01245-14 (2014).
96. M. H. Larsen, K. Biermann, S. Tandberg, T. Hsu, W. R. J. Jacobs, Genetic manipulation of *Mycobacterium tuberculosis*. *Curr. Protoc. Microbiol.* **6**, 10A.2.1–10A.2.21 (2007).
97. L. Wang *et al.*, *Mycobacterium tuberculosis* massive gene amplification to overcome loss of ESX-3 secretion system substrates. National Center for Biotechnology Information. <https://www.ncbi.nlm.nih.gov/bioproject/PRJNA784324>. Deposited 28 November 2021.